CHAPTER 3

Start-to-End Beam Dynamics Simulation

Properties of radiation from charged particle beam depend significantly on the beam quality. In this chapter, a gradient of an alpha magnet, an energy cut condition by using energy slits inside the alpha magnet vacuum chamber, and an RF-phase of the linac were optimized to obtain the shortest electron bunch length, the maximum number of electrons per bunch, and the lowest energy spread at the experimental station. Furthermore, the strengths of quadrupoles and steerers were adjusted to achieve small transverse beam size and divergence, which result in small emittance. These longitudinal and transverse beam properties are crucial for producing the coherent undulator radiation with high intensity and brightness.

In this study, we concentrated on the electron beam dynamics from the RF-gun to the experimental station that is divided into three parts. The first part is inside the RF-gun. The second part is from the gun exit to entrance of the alpha magnet (GTA). The last part is from the alpha magnet to the experimental station (ATE). All beam dynamics simulation described in this chapter was done by using the program PARMELA except the simulation inside the alpha magnet, which was performed by using the program ELEGANT. Simulation algorithms for these three parts are shown in Fig. 3.1.

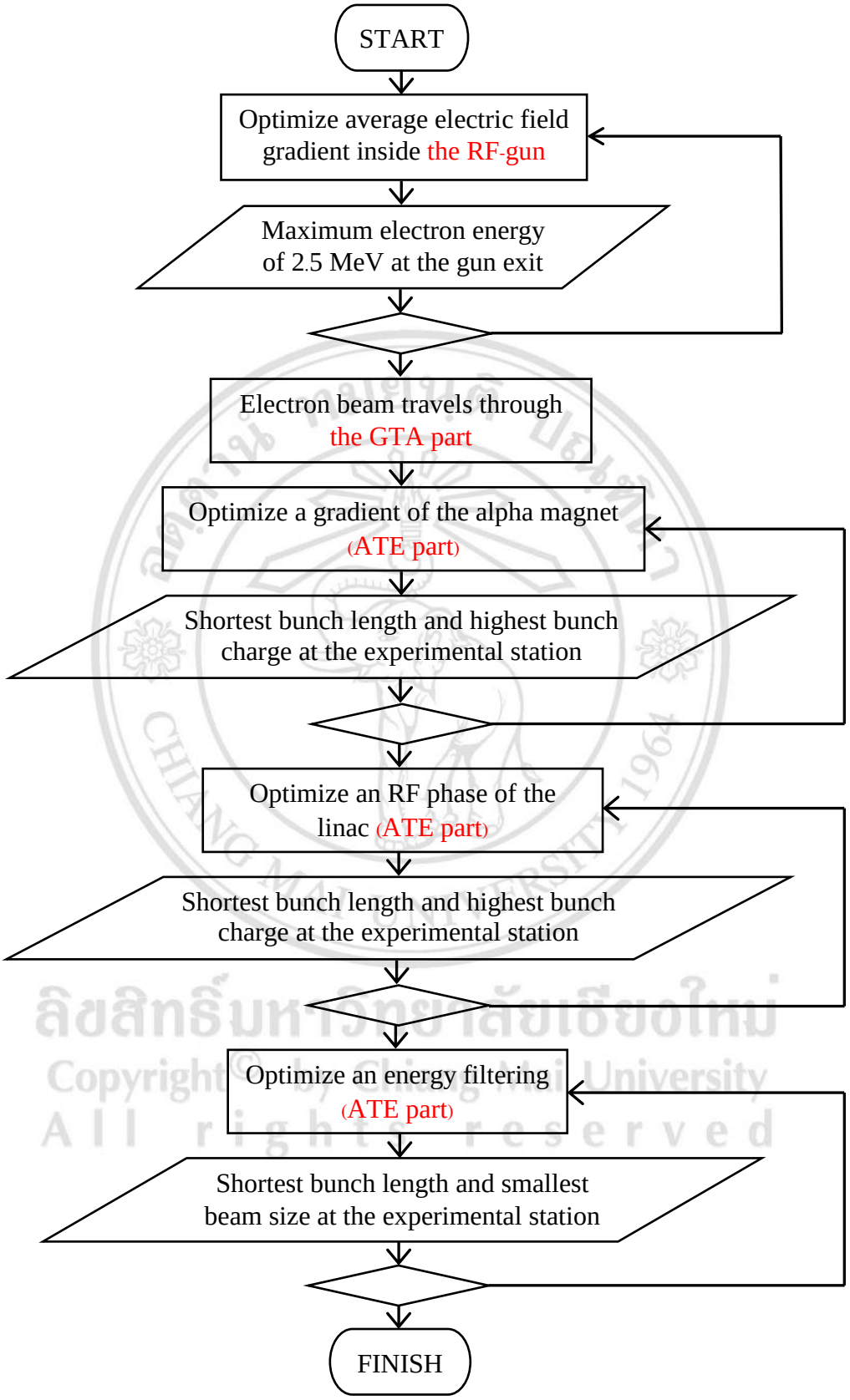

Figure 3.1: Flowchart of simulation algorithms of beam dynamics simulation.

3.1 Electron Beam Dynamics Simulation inside the RF-gun

The electron beam dynamics inside the RF-gun was simulated by using program PARMELA. The electric field amplitude inside the gun was optimized in order to achieve the electron bunch with the maximum kinetic energy of 2.5 MeV according to the measurement result. Practically, the maximum accelerating electric field strength is constrained by the breakdown and the back-bombardment effect [5]. The 6-mm diameter flat cathode was employed in the beam dynamics simulation. Electrons with no energy spread and non-zero emittance are emitted uniformly from the cathode surface with the average current of 2.6A over an RF period. A normalized thermal emittance of 2.78 mm.mrad and a kinetic energy of 0.165 eV were defined for the initial emitted electrons. These values are associated with a cathode temperature of 1000℃. An initial number of macro-particles, which represents the group of the electrons, is 250,000 macro-particles corresponding to a total charge of 976 pC. Thus, one macro-particle has a charge of 3.9 fC. The space charge calculation was included with the radial and longitudinal mesh intervals of 40 and 2000, respectively. The initial number of macro-particles and the number of mesh intervals for beam dynamic simulation from the RF-gun to entrance of an alpha magnet were optimized and presented in the reference [34]. The Schottky effect and the electron back-bombardment were not considered in this simulation. Furthermore, we applied the 3D electromagnetic field distribution of the RF-gun obtained from the program CST Microwave Studio (MWS) 2012 in the simulation [9]. The electric field parameters used in this simulation are listed in Table 3.1 and the electric field vectors inside the RF-gun are shown in Fig. 3.2. Both the side-coupling cavity and the RF waveguide input port lead to asymmetric electromagnetic field distribution in both horizontal and vertical directions inside the gun cavities.

Table 3.1: The electric field parameters of the PBP-CMU gun obtained from the results of the 3D MWS model [9].

Parameter	Value
Average field in half cell	24.18 MV/m
Maximum field in half cell	31.43 MV/m
Average field in full cell	39.88 MV/m
Maximum field in full cell	63.27 MV/m
Average field ratio	1.65
Maximum field ratio	2.01

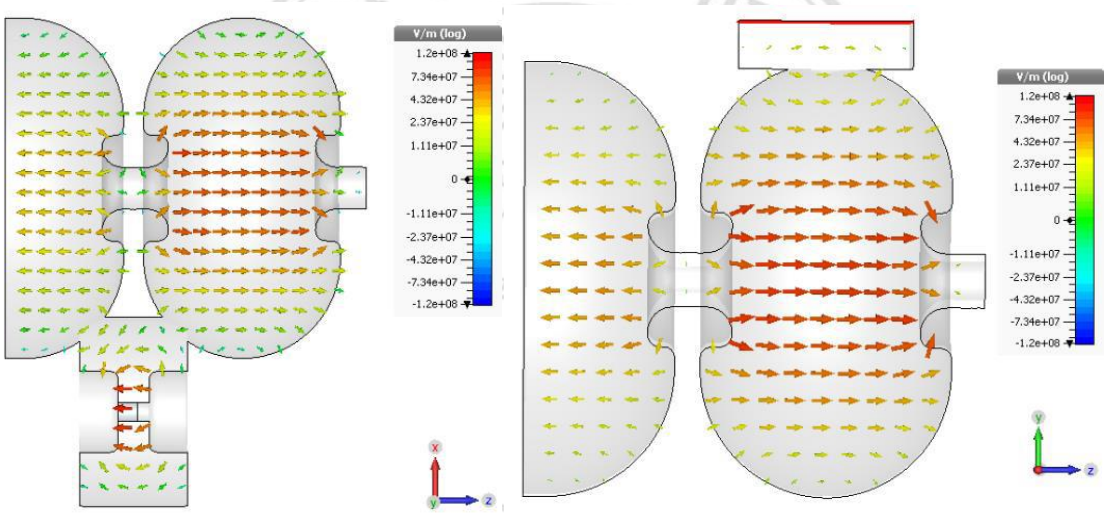

Figure 3.2: Electric field vectors inside the RF-gun for the horizontal plane (left) and for the vertical plane (right) [9].

The simulation results of electric field variation are shown in Fig. 3.3 - 3.4. Obviously, the electrons emitted from the thermionic cathode gain higher energy for higher average electric field. The energy spread of the electron beam exiting the RF-gun is high due to time-varying feature of the RF accelerating field. This leads to the large energy difference between high and low energy electrons in the bunch. The maximum electron energy reaches 2.5 MeV at the average field gradient of 41.7 MV/m.

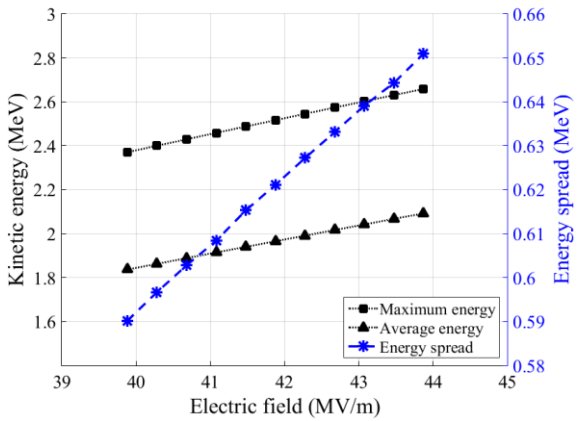

Figure 3.3: Dependency of average and maximum energy (vertical left axis) and energy spread (vertical right axis) of electron beam at the gun exit as a function of average electric field at the center of the full cell.

Divergence angles of lower energy electrons leaving from the RF-gun are larger than that of higher energy electrons. Thus, electrons with low kinetic energies lead to the large transverse divergence of the whole bunch at the gun exit. As shown in Fig. 3.4, when the average electric field gradient inside the gun increases, the micro-bunch charge at the gun exit increases resulting in larger Coulomb's force. Consequently, the rms transverse beam size increases. However, the rms divergence reduces due to the focusing from the RF field. Moreover, Fig. 3.4 (right) indicates that at higher electric field gradient, more electrons can depart from the RF-gun.

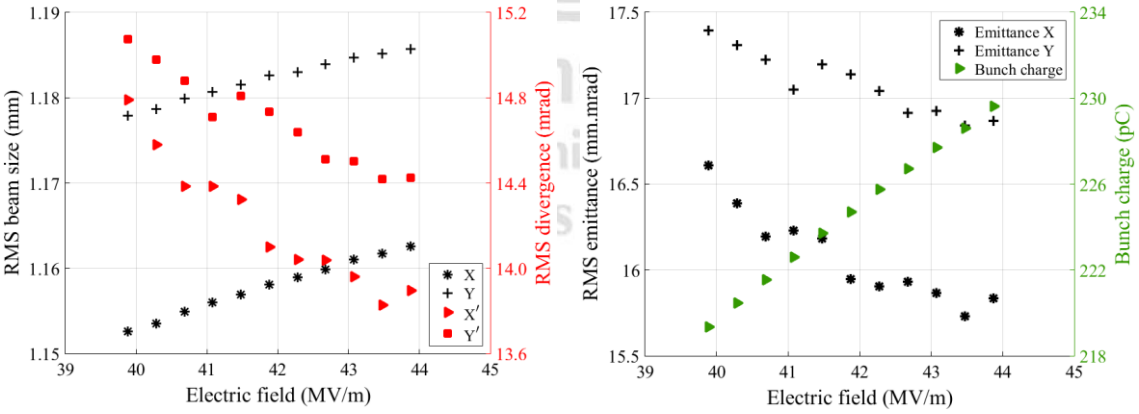

Figure 3.4: RMS transverse beam size and divergence as a function of the average electric field at the full-cell center (left). The rms emittance and the micro-bunch charge of electron beam exiting the RF-gun as a function of the average electric field at the full-cell (right).

The transverse beam distributions as shown in Fig. 3.5 shows that the centroid position of the electron bunch at the gun exit is off-axis by 0.280 mm and -0.024 mm for horizontal and vertical directions, respectively. This is due to the influence of the kick from the asymmetric field distribution inside the gun cavities [9]. The transverse phase space distributions for both planes are butterfly-like shapes that have the high charge intensity at the divergence close to zero. At the RF-gun exit, electrons with high kinetic energy are accommodated at the head of the bunch. Smaller fraction of electrons in the tail of the bunch has lower kinetic energy. Such a longitudinal particle distribution is suitable for the bunch compression using the alpha magnet.

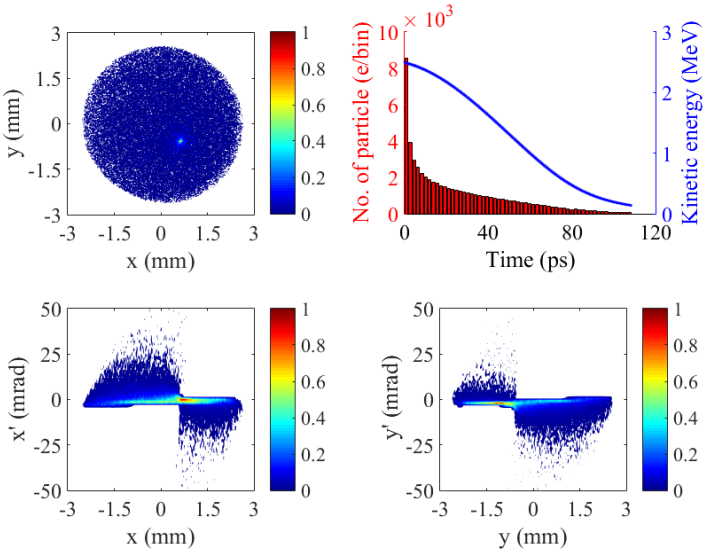

Figure 3.5: Contour plots of transverse beam distribution (x-y), longitudinal phase space distribution (E_k-t) with histogram of the number of macro-particles at the RF-gun exit and transverse phase space distributions (x-x′ and y-y′).

The electron beam with a bunch charge of 224 pC after exiting the RF-gun was classified by particles' kinetic energies and plotted in Figs. 3.6 - 3.7. The number of particles with kinetic energy in the range of 2 to 2.5 MeV are 66% of the total particles in the bunch. The low-energy electrons at the tail of the bunch have smaller transverse displacements and locates off-axis than the high-energy electrons. Electrons with nearly zero divergence have high kinetic energy. The rms beam sizes in x and y axes are 1.16 mm and 1.18 mm with the average energy of 2 MeV and the energy spread of 0.62 MeV. The transverse beam emittances are 16.09 mm.mrad and 17.25 mm.mrad for x and y directions, respectively.

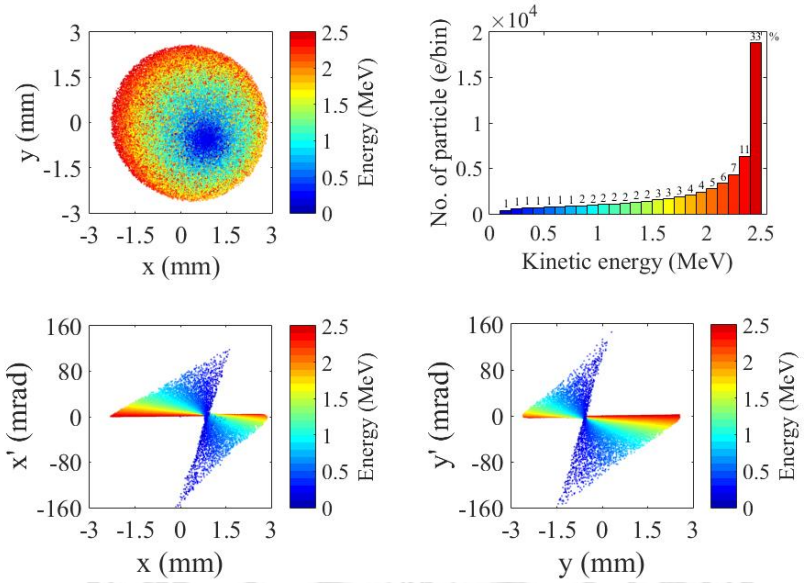

Figure 3.6: Transverse distribution (x-y), energy spectrum and transverse phase space distributions (x-x′ and y-y′) at the RF-gun exit. Different colors in the plots represent different particle energies.

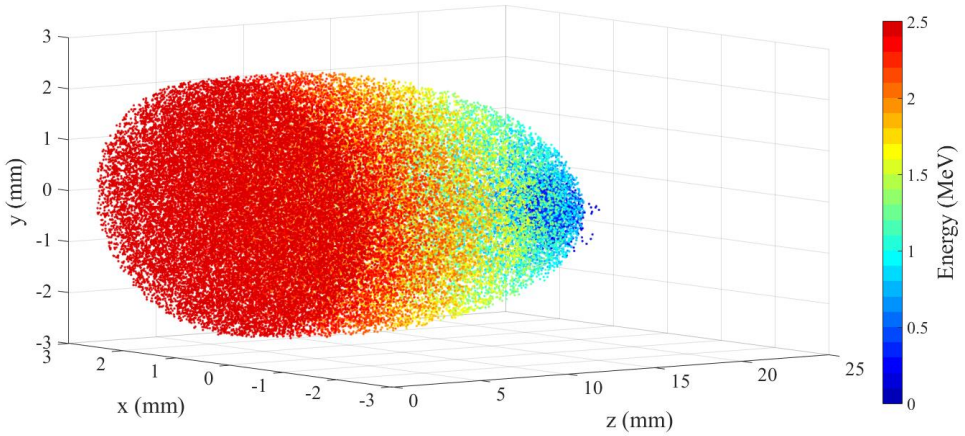

Figure 3.7: Three-dimensional electron beam distribution at the RF-gun exit.

3.2 Beam Dynamics Simulation from RF-gun Exit to Alpha Magnet Entrance (GTA)

In this part, we considered the electron trajectory from the gun exit to the alpha magnet entrance **(**GTA**)** and simulated the beam dynamics in three situations**.** Firstly, the simulation in the GTA part was performed without defining the boundary of vacuum chamber**.** Thus, the electron bunch travels in an infinite vacuum space**.** Secondly, we considered that the electron bunch moving along the GTA section with a specific

vacuum boundary. The aperture radius of the vacuum chambers along the PBP-CMU beamline is different as listed in Appendix. In this case, there was no quadrupole or steering magnetic field applied. Thirdly, the beam dynamics were simulated with vacuum chamber boundary and the electron beam trajectory in the GTA part was controlled by using quadrupole and steering magnets.

The steering magnets were used to keep electrons close to the centroid position of the vacuum tube at a desired location. The steering magnet with high magnetic field, which is used to steer the electron beam, causes the enlargement of the transverse divergence and emittance downstream that magnet. Consequently, the electron beam is then off-center again when it travels away from the magnet. Thus, we used more than one steering magnet in the beam transport line in order to slightly adjust the electron beam trajectory. The quadrupole magnet is a focusing element, which is used to control the transverse size and divergence of the electron beam passing through the beamline. However, the electrons' trajectories lengthen when using the quadrupole magnet. As a result, electron bunch length is increased. Hence, careful quadrupole magnetic field adjustment is required in electron beam transportation along the accelerator system.

The electron beam leaving from the RF gun was directed to the center of the screen station 1 (SC1) by using a steering magnet 1 (ST1). All steering magnets in the GTA section combines two small dipole magnets for steering in horizontal and vertical directions. Three quadrupoles (Q1, Q2, Q3) were used to minimize the transverse size and divergence of the electron beam in order to prevent the main part of the beam to hit the vacuum chamber wall. Then, the electron beam was guided to the center of the alpha magnet entrance with small divergence by using the steering magnet 2 (ST2). If the electron beam enters the alpha magnet with large divergence, the main part of the beam will depart from the alpha magnet with off-axis centroid position contributing to emittance growth and bunch length enlargement [35].

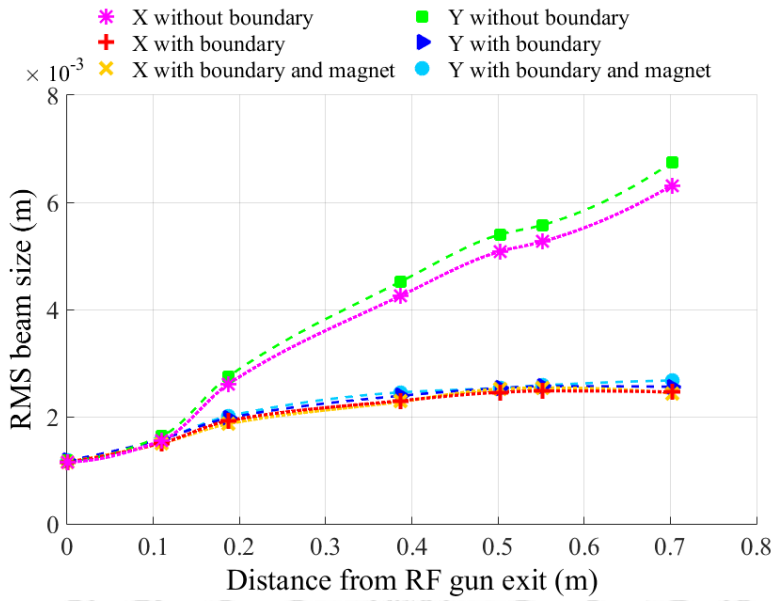

Figure 3.8: RMS transverse beam size along the GTA section for different simulation conditions. The data points in the graphs represent the positions of the RF-gun exit, ST1, Q1, Q2, Q3, ST2, and the alpha magnet entrance, respectively.

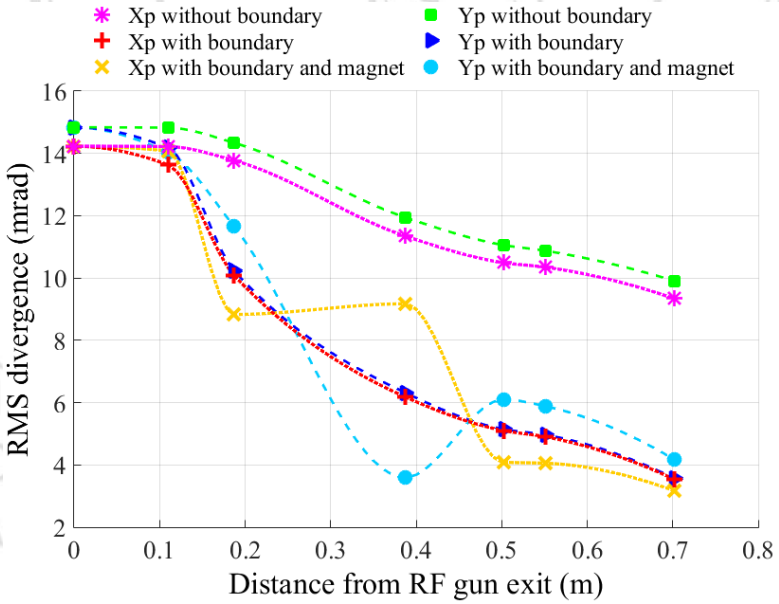

Figure 3.9: Divergence of electron beam along the GTA beamline for different simulation conditions.

Figures 3.8 - 3.12 display the rms transverse beam size, divergence, beam emittance, average kinetic energy, energy spread and bunch charge along the GTA section for three cases of beam dynamic simulation. The results from the simulation without boundary of vacuum chamber shows that the rms transverse beam size increases along the GTA section because the electron beam leaves from the RF-gun with a specific converging angle. The divergence values in both horizontal and vertical directions reduce when the distance from the gun exit increases. The electron beam size enlarges to be bigger than the vacuum boundary and the beam starts to collide with the chamber wall at the ST1 position. The electron beam sizes in the simulation cases with the vacuum boundary are hence limited by the size of the chamber aperture.

The number of electrons hitting the chamber wall increases from the position of ST1 (at the position of 0.11 m from the gun exit) to the alpha magnet entrance causing the reduction of the electron bunch charge as shown in Fig. 3.12. The lost electrons are the ones with high divergent angles and low kinetic energies. Thus, the transverse divergence and the energy spread in the simulation with the vacuum boundary decrease. As the results, the transverse emittance and the average beam energy in these two cases increase.

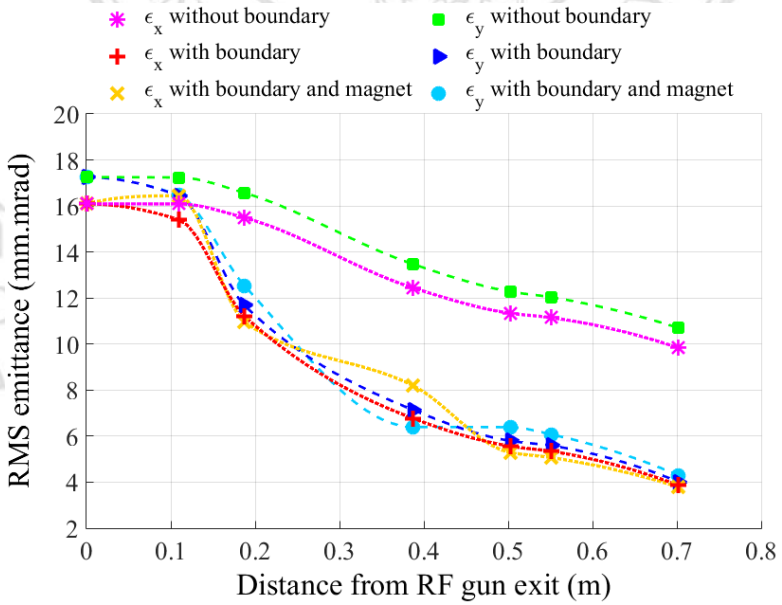

Figure 3.10: RMS transverse emittance along the GTA section for 3 conditions of beam dynamic simulation.

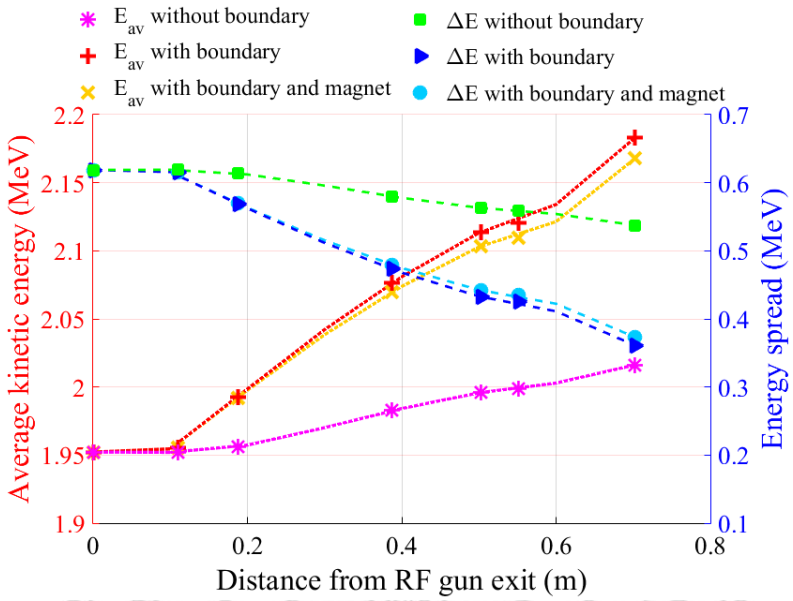

Figure 3.11: Average kinetic energy and energy spread along the GTA section for 3 cases of beam dynamic simulations.

When quadrupole and steering magnets are used, we are able to reduce the number of electrons, which hit the vacuum chamber wall. Thus, the bunch charge at each position for this simulation is higher than that of the simulation without the magnet as illustrated in Fig. 3.12. Consequently, the beam energy spread for simulation with the magnets are higher due to more contribution from low-energy electrons.

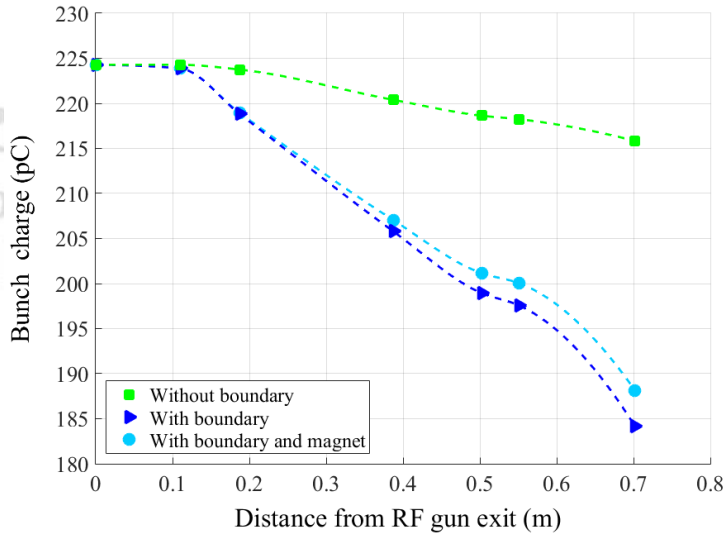

Figure 3.12: Electron bunch charge at the positions of the elements along the GTA part for different conditions of beam dynamic simulation.

The transverse and longitudinal distributions of the electron beam for the simulation with vacuum boundary and magnets are shown in Figs. 3.13 - 3.15. This simulation condition was then applied to all beam dynamics mentioned later in this study. The electron beam with the bunch charge of 188 pC at the alpha magnet entrance has the transverse size in x-axis of 2.44 mm and y-axis of 2.67 mm. It has a maximum kinetic energy of 2.2 MeV and an energy spread of 0.37 MeV. The energy-time distribution in Fig. 3.13 reveals that high-density electron fraction is at the head of the bunch with a length of a few tenth picoseconds. In addition, the bunch length increases compared to the electron bunch at the gun exit due to the effect of the electrons' movement with large energy spread and non-zero divergence. The horizontal and vertical transverse emittances are 4.39 and 4.30 mm.mrad, respectively.

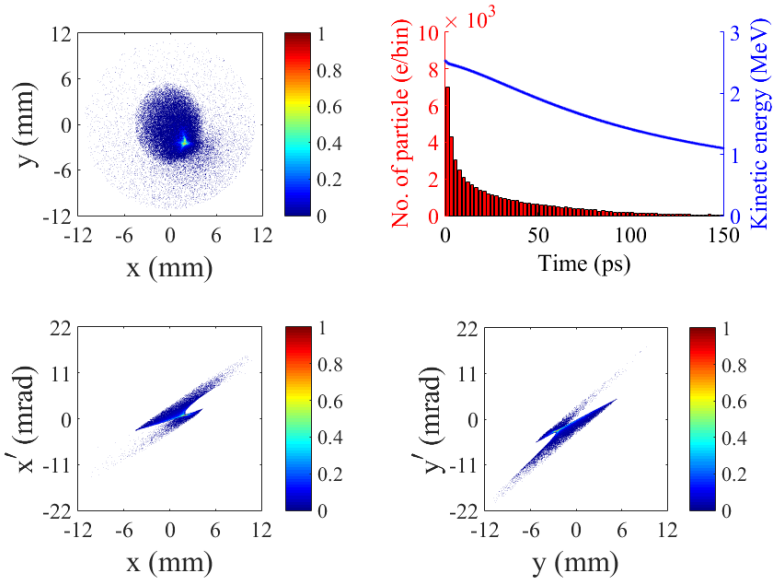

Figure 3.13: Transverse beam distributions (x-y), the energy-time phase space (E_k-t) with histogram and transverse phase space distributions (x-x′ and y-y′) of electron bunch at the alpha magnet entrance. Different colors in the plots represent different particle intensities in arbitrary unit.

High-energy electrons were directed to the center of the vacuum chamber at the alpha magnet entrance. The electron fraction with energy lower than 2 MeV, which is located at the tail of the bunch and has large transverse displacement, was steered off from the center of the vacuum chamber and lost at the chamber wall. The electrons with energy lower than 1 MeV are also lost along the GTA section. The distributions with

energy classification at the alpha magnet entrance are shown in Fig. 3.14. The electrons at the center of the transverse distribution have smaller divergence angle than the outer electrons. The 3D beam distribution in Fig. 3.15 illustrates that the waist of the longitudinal electron bunch at the kinetic energy of around 2.1 MeV.

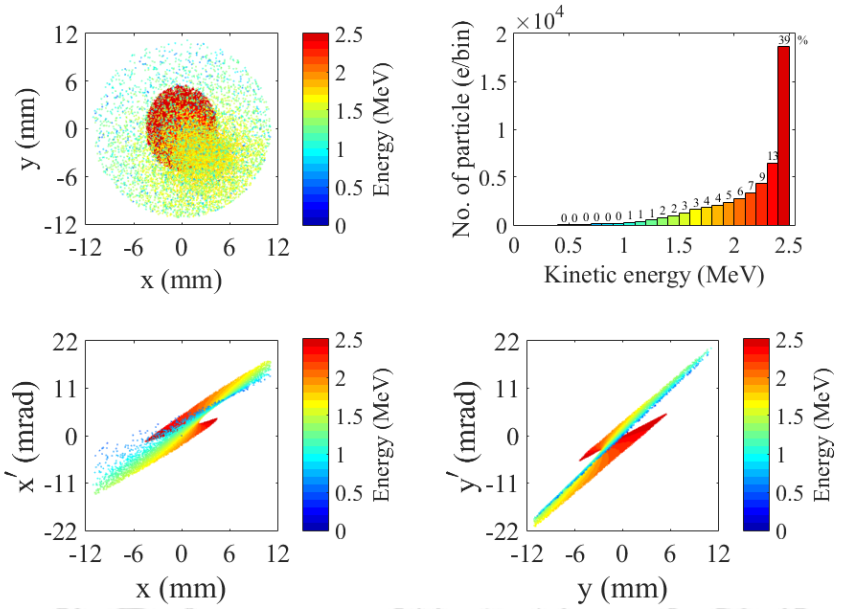

Figure 3.14: Transverse distribution (x-y), energy spectrum and transverse phase space distributions (x-x′ and y-y′) with energy classification at the alpha magnet entrance. Different colors in the plots represent the particles with different energies.

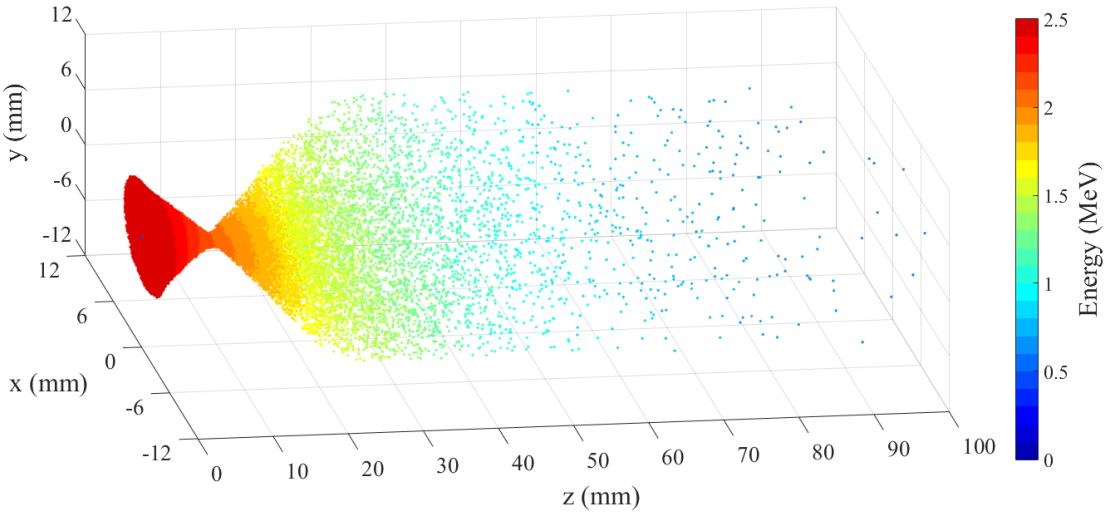

Figure 3.15: Three-dimensional electron beam distribution with energy classification at the alpha magnet entrance.

3.3 Beam Dynamics Simulation from Alpha Magnet to Experimental Station (ATE)

The electron beam traverses into the alpha magnet with an angle of 49.29° with respect to the magnet axis. The electron's trajectory (s_{max}) in the alpha magnet depends on the electron momentum ($\beta\gamma$) and the magnetic field gradient (g) as explained in Chapter 2. The electron with lower momentum travels with shorter path length in this magnet than the path length of the larger momentum electron. Therefore, the alpha magnet can be used as a magnetic bunch compressor for low energy beams with well correlation between energy and time. After exiting the alpha magnet, the transverse properties of electron beam are controlled by the quadrupoles Q4 - Q5 and the steering magnets ST3 and ST4. The beam is directed to enter the linac at the centroid position with nearly zero divergence. Electrons in the bunch are accelerated in the linac with slightly different phases depending on their positions in the bunch. Thus, the magnetic field gradient of the alpha magnet has to be adjusted corresponding the desired accelerating phase of the linac. Then, the accelerated electrons exit the linac and continuously move through the quadrupoles Q6 and Q7 toward the experimental station for generating the undulator radiation.

The electron beam with short bunch length, high bunch charge, low energy spread, and low transverse emittance is preferred for producing the high-brightness, narrow-band and coherent THz undulator radiation. The alpha-magnet gradient, the energy filtering condition using the alpha magnet energy slits and the linac RF phase were considered and varied to optimize the electron beam properties. The accelerating electric field of the linac was set to obtain the average electron beam energy of around 9.81 MeV (based on the measurement value) at the experimental station. The magnetic field strengths of all quadrupoles and steering magnets were adjusted simultaneously corresponding to each set of operating parameters.

3.3.1 Beam Dynamics Simulation in Alpha Magnet

Since program PARMELA does not support the simulation in the alpha magnet, the six-dimensional electron beam distributions at the alpha magnet entrance obtained from PARMELA simulation as described in section 3.2 were converted to be the

appropriated format for ELEGANT input. Table 3.2 shows comparison of the particle distribution formats using in programs PARMELA and ELEGANT.

Table 3.2: Comparison of particle distribution formats for programs PARMELA and ELEGANT.

Parameter	PARMELA	ELEGANT
Horizontal displacement	x (cm)	x (m)
Horizontal angular displacement	x' (mrad)	x' (rad)
Vertical displacement	y (cm)	y (m)
Vertical angular displacement	y' (mrad)	y' (rad)
Longitudinal displacement	*phi* (degree)	t (s)
Particle energy	kinetic energy: w (MeV)	momentum: $\beta\gamma$ (p/m_0c)

The maximum distance in x direction ($xmax$) of electron trajectory is used to determine the alpha magnet gradient (g) in the code ELEGANT. The dependence of the two parameters follows equation (2.35) in Chapter 2. The alpha magnet transfer matrix can be used with first to third orders. The electron beam exiting the alpha magnet with higher order matrix has larger transverse divergence resulting in increasing of electron beam size along the beamline. This is due to the effect of coupled magnetic fields in transverse plane. When the electron beam with high divergence value is accelerated and departs from the linac, the transverse beam size is exceeding the vacuum chamber dimension. Then, the quadrupoles Q4 and Q5 located upstream the linac cannot be used to focus the electron beam to have a transverse size smaller than the vacuum chamber aperture at the linac exit. This is not corresponding to the measured beam transverse size at the linac exit that is smaller than the vacuum chamber aperture. Consequently, the first order transfer matrix of the alpha magnet was applied for the ELEGANT simulation. As an example, the electron beam distributions at the alpha magnet exit for the magnetic field gradient of 328 G/cm are shown in Figs. 3.16 - 3.18.

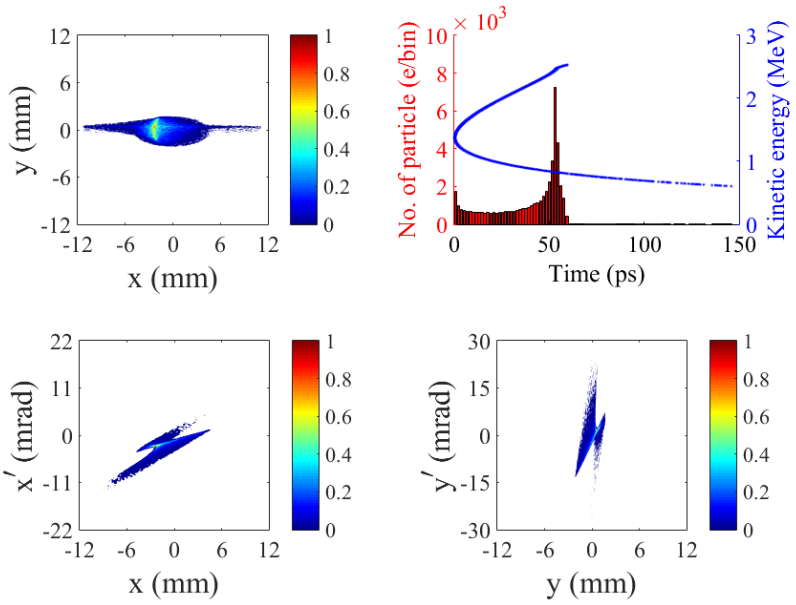

Figure 3.16: Contour plots of transverse beam distribution (x-y), the energy-time phase space (E_k-t) with histogram and transverse phase space distributions (x-x′ and y-y′) of electron beam at the alpha magnet exit for the magnetic field gradient of 328 G/cm. Different colors in the plots represent different particle intensities in arbitrary unit.

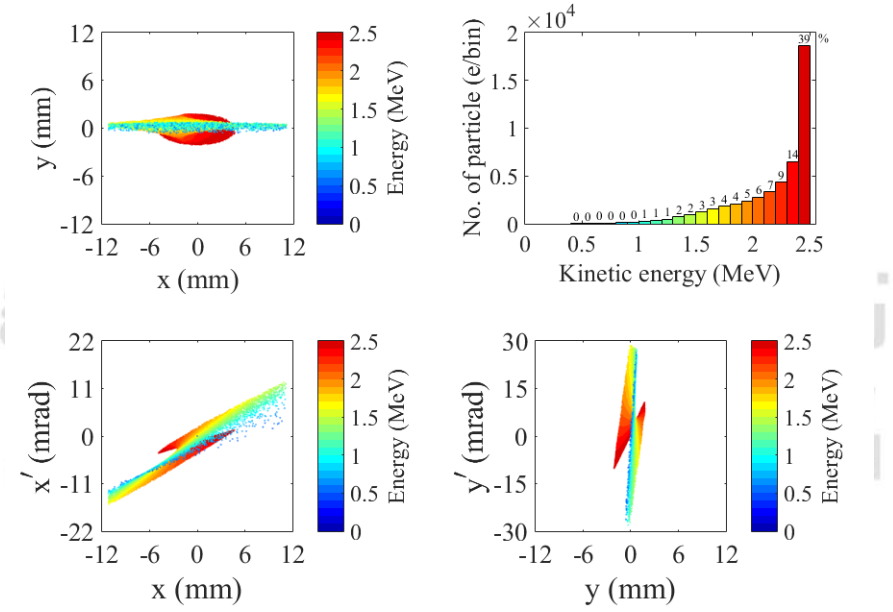

Figure 3.17: Transverse distribution (x-y), energy spectrum and transverse phase space distributions (x-x′ and y-y′) with energy classification at the alpha magnet exit for the magnetic field gradient of 328 G/cm. Different colors in the plots represent the particles with different energies.

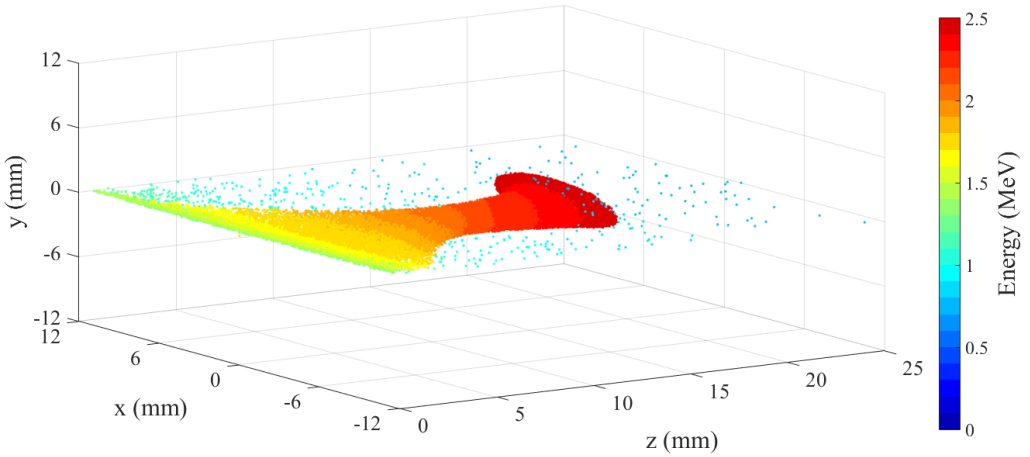

Figure 3.18: Three-dimensional electron beam distribution with energy classification at the alpha magnet exit for the magnetic field gradient of 328 G/cm. Different colors in the plots represent the particles with different energies.

3.3.2 Optimization of Longitudinal Mesh for Simulation in ATE Section

Longitudinal and radial mesh sizes are significantly associated with calculation of space-charge field in PARMELA simulation. The maximum radial mesh number of 30 [23] was applied for the transverse radius of 1.27 cm. Then, the number of longitudinal mesh was optimized. The considered electron beam properties are bunch length, energy spread and emittance. The electron bunch length at the experimental station was determined in terms of rms bunch length, FWHM bunch length and Gaussian fitting bunch length.

The longitudinal mesh number was varied from 200 - 3000 in the distance of 16cm. The alpha magnet gradient of 328 G/cm was used according to the experimental value. The linac RF phase was set to 90°. The optimization was done without using energy filters in the alpha magnet. The bunch length, energy spread, and transverse emittance of electron beam traveling to the experimental station are displayed in Fig. 3.18.

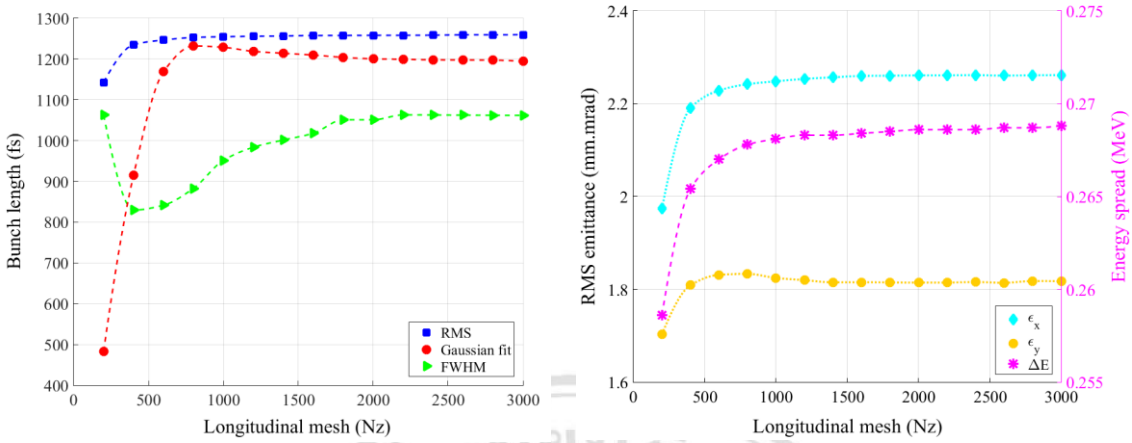

Figure 3.19: Bunch length, rms transverse emittance and energy spread of electron beam at the experimental station for different numbers of longitudinal mesh interval.

The values of electron bunch length are nearly constant when the longitudinal mesh number is greater than 1800. The energy spread and the transverse emittance start to be constant when the longitudinal mesh is greater than 1200 and 1600, respectively. Therefore, the appropriated number of longitudinal mesh for simulation in the ATE part is 1800, while the number of radial mesh is 30.

3.3.3 Optimization of Alpha Magnet Gradient

In this optimization, the alpha magnet gradient was initially varied from 100 G/cm to 700 G/cm without using the energy filters. The RF phase of the linac was set to be at 90° corresponding to the on-crest or the maximum acceleration condition. The longitudinal phase space of the electron beam at the alpha magnet entrance as shown in Fig. 3.13 is properly compressed by the magnetic field of the alpha magnet. High-energy electrons at the head of the bunch enter firstly to the alpha magnet and travel with longer path lengths than lower energy electrons positioned at the tail of the bunch. Eventually, some low-energy electrons are able to catch up the high-energy electrons and depart earlier from the alpha magnet. Thus, the longitudinal phase spaces of electron bunches at the alpha magnet exit are clockwisely rotated as shown in Figs. 3.20 and 3.21. This leads to proper bunch compression of the electron beam at the experimental station.

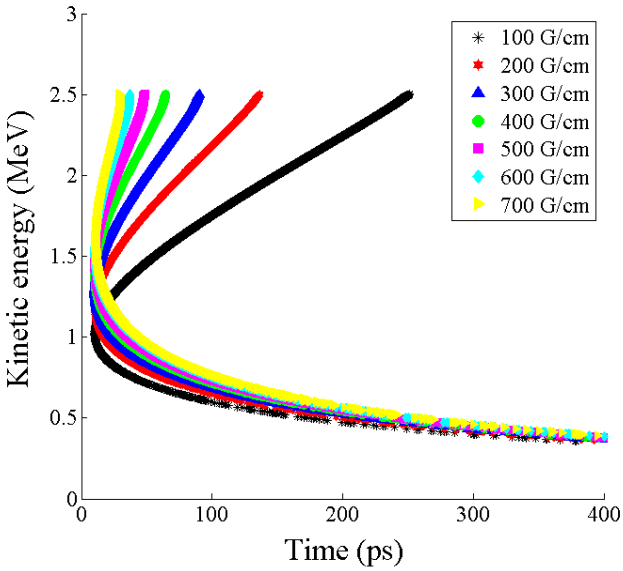

Figure 3.20: Energy-time distributions at the alpha magnet exit for magnetic field gradients of 100 - 700 G/cm.

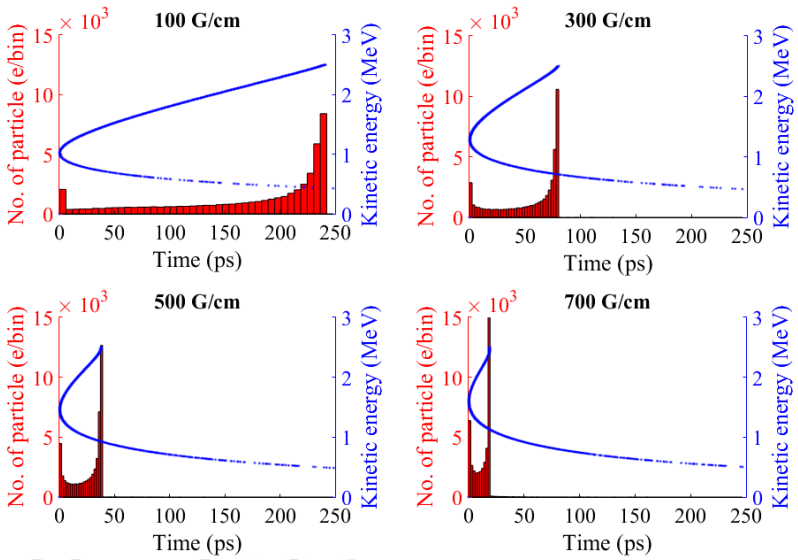

Figure 3.21: Histograms of the electron bunches at the alpha magnet exit for alpha magnet gradients of 100, 300, 500, 700 G/cm.

Figures 3.20 and 3.21 reveal that only partial electron beam distribution at the head of the bunch is compressed and rotated by the magnetic field of the alpha magnet. For all alpha magnet gradients, the electrons at the tail of the bunch with very low momenta have very short path length and travel through the alpha magnet with almost the same distance due to the exponential relation of the electron momentum and the path

length in the alpha magnet. The electron trajectory in the alpha magnet shortens when the alpha magnet gradient increases causing the so-called over-compression. The under-compression condition of the longitudinal phase space occurs when using the low alpha magnet gradient.

The effect of alpha magnet gradient to the transverse beam characteristics at the alpha magnet exit is presented in Fig. 3.22. The magnetic field of the quadrupoles and the steering magnets play a significant role in the transverse beam properties. Hence, the field strengths of the whole magnets in the GTA section were optimized to proper values for different gradients of the alpha magnet.

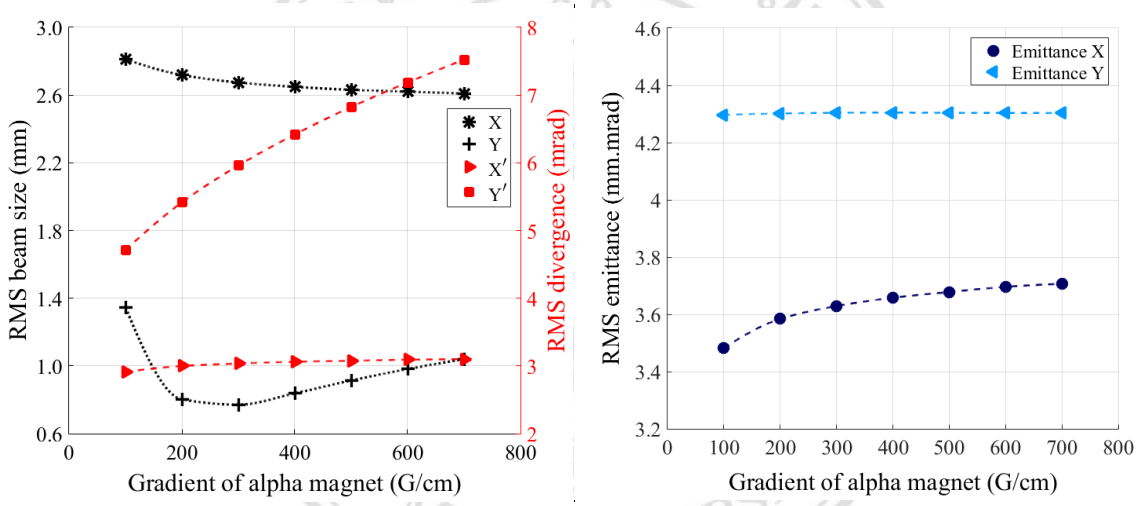

Figure 3.22: RMS transverse beam size, divergence and rms transverse emittance at the alpha magnet exit as a function of the alpha magnet gradient.

The electron bunch is focused in the vertical direction after moving through the magnetic field of the alpha magnet. The beam size in y axis is minimum when the alpha gradient is 300 G/cm as shown in Fig. 3.22. Transverse and phase space distributions of electron bunch at the alpha magnet exit for the alpha magnet gradients of 100 - 400 G/cm are shown in Fig. 3.23. The phase-space rotation from the converging beam to be the diverging beam starts when the alpha magnet gradient is larger than 300 G/cm. This results in increasing of the divergence value and large emittance in vertical direction. Contradictory, the beam size, divergence and emittance in horizontal direction do not change much for different alpha magnet gradients.

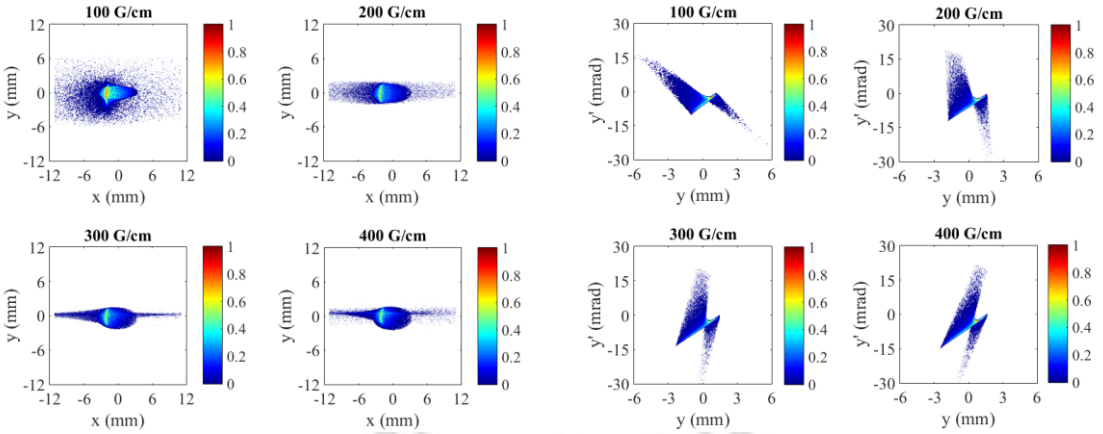

Figure 3.23: Transverse distribution (x-y) and transverse phase space (x-x′ and y-y′) of electron bunches exiting from the alpha magnet for the alpha magnet gradients of 100, 200, 300, and 400 G/cm.

The electron beam distribution at the alpha magnet exit simulated from program ELEGANT was transformed to have appropriated PARMELA input format for simulation in the ATE section**.** The reference particle is not determined for ELEGANT simulation**.** Thus, we have to choose a reference particle in a bunch for the input beam distribution in PARMELA simulation**.** Longitudinal phase space distributions of electron bunches at the linac entrance for different alpha magnet gradients without using energy filters are shown in Fig 3.24**.**

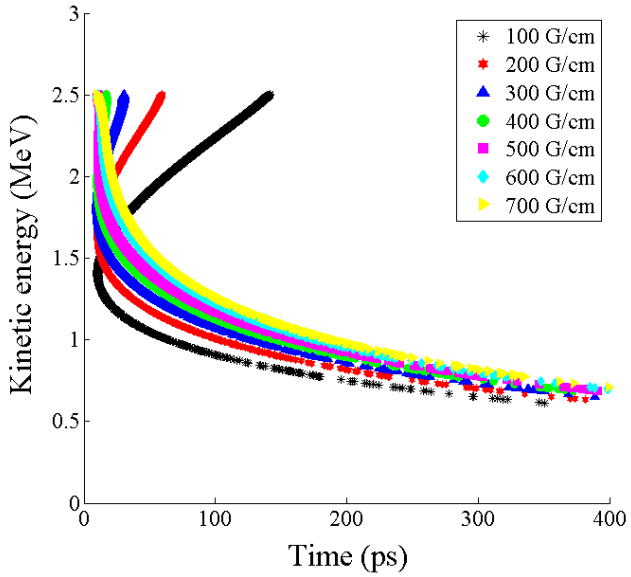

Figure 3.24: Longitudinal phase space distributions of electron bunches at the linac entrance for alpha magnet gradients of 100 - 700 G/cm.

The bunch length of the electron beam moving from the alpha magnet exit to the linac entrance shortens due to the difference of particles' velocities. The high-energy electrons located at the tail of the bunch catch up the low-energy electrons before entering the linac. Therefore, optimization of the alpha magnet gradient to compensate the different path lengths due to velocity dispersion of electron beam was performed in order to achieve a shortest electron bunch at the experimental station. Figure 3.25 shows the longitudinal phase space distributions of electron bunches at the experimental station for different alpha magnet gradients. Energy-time distributions and histograms of electron beams at the experimental station for the alpha magnet gradients of 100 - 600 G/cm are shown in Fig. 3.26.

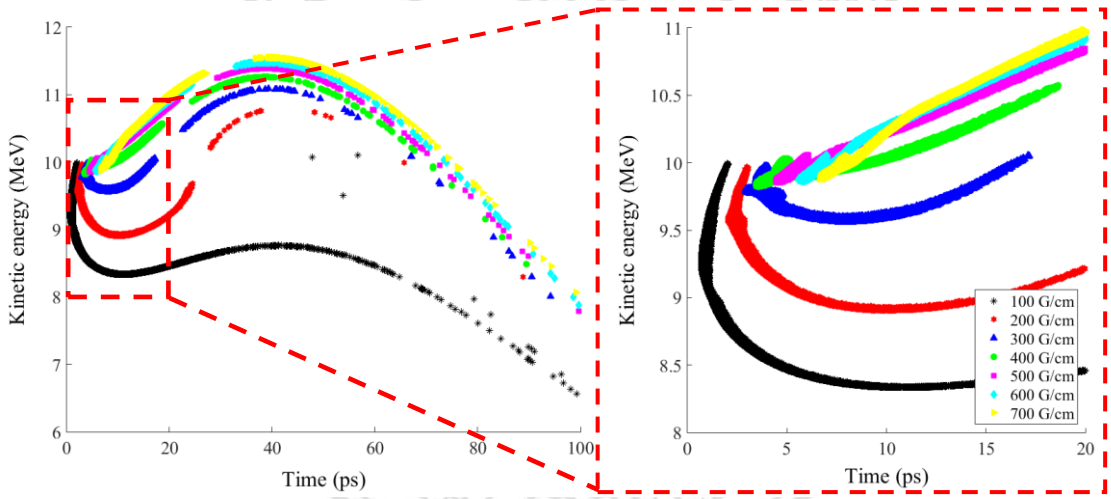

Figure 3.25: Longitudinal phase space distributions of electron bunches arriving at the experimental station for alpha magnet gradients of 100 - 700 G/cm.

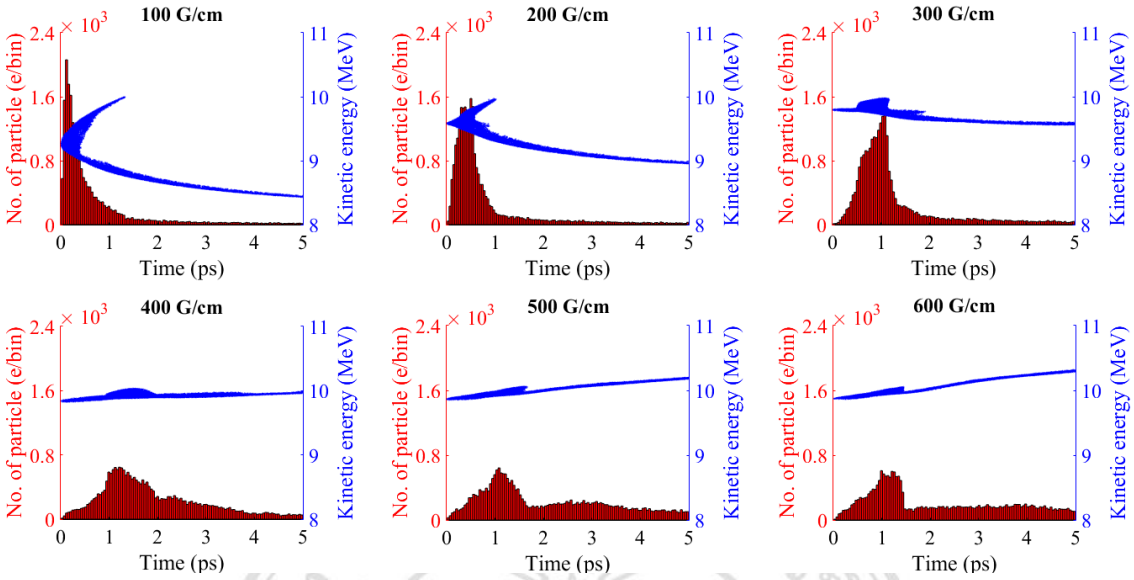

Figure 3.26: Energy-time distributions and histograms of electron bunches at the experimental station for alpha magnet gradients of 100 - 600 G/cm.

Electrons concentrated in the head of the bunch have various longitudinal beam characteristics for different alpha gradients. As shown in Fig. 3.26, energy-time phase spaces for alpha magnet gradients of 100 and 200 G/cm are under-compressed and have high charge intensity at the first few picoseconds at the head of the bunch. For any alpha magnet gradient greater than 400 G/cm, the number of electrons accumulated at the head of the bunch decreases and the longitudinal phase space is over-compressed. Therefore, the optimum compression of the longitudinal phase space at the experimental station should be obtained when the alpha magnet gradients are in the range of 200 - 400 G/cm.

In this study, the electron bunch length is determined in three definitions; the statistic rms bunch length, the FWHM bunch length and the Gaussian fitting width. The Gaussian fitting width will properly be a good representation of the longitudinal length for the electron bunch when the R-squared value of the fitting is close to unity.

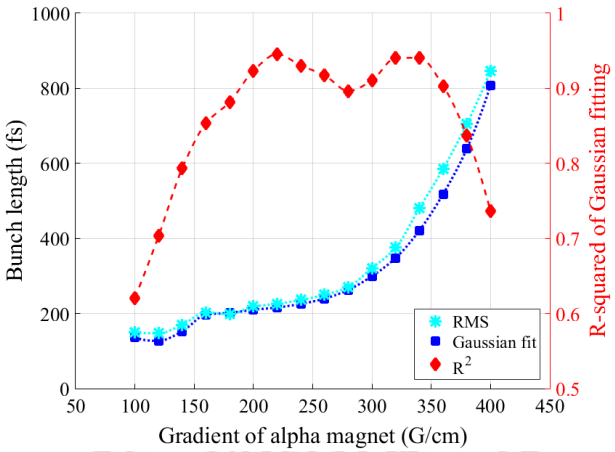

Figure 3.27: RMS and Gaussian fitting bunch lengths at the experimental station for alpha magnet gradients of 100 - 400 G/cm. The right vertical axis shows the R-squared value of the Gaussian fitting for each gradient.

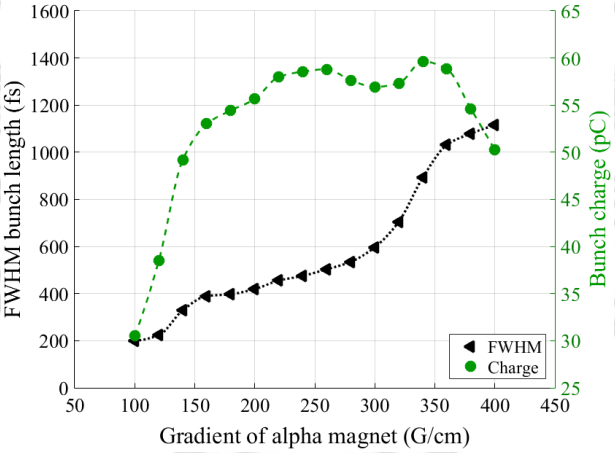

Figure 3.28: FWHM bunch length (left vertical axis) and micro-bunch charge (right vertical axis) at the experimental station for alpha magnet gradients of 100 - 400 G/cm.

The simulation results in Figs. 3.27 and 3.28 show that the electron bunch lengths for all three definitions increase as the gradient of the alpha magnet is raised. The rms bunch length is comparable to the Gaussian fitting bunch length, while the FWHM bunch length is about two times larger. This is quite corresponding to the definition of the FWHM width and the rms width of the Gaussian distribution [36]. However, there is some differences from this definition at the alpha magnet gradients lower than 200 G/cm and higher than 360 G/cm where the particle longitudinal distributions are not close to Gaussian distribution. The R-squared value of the Gaussian fitting and the bunch charge are maximum in the range of the alpha magnet gradient

between 200 - 360 G/cm. In this gradient range, the rms and the Gaussian fitting bunch lengths are about 200 - 600 fs, while the FWHM bunch length is about 400 - 1000 fs. The electron bunch charge is 55 - 60 pC. It can be preliminary concluded that the optimal alpha magnet gradient to achieve the electron beam with high bunch charge and short bunch length at the experimental station should be in the range of 200 to 400 G/cm.

3.3.4 Optimization of Linac RF Phase

As an example, three-dimensional distribution, transverse distribution, energy spectrum and energy-time phase space of electron bunch at the linac entrance for the alpha magnet gradient of 300 G/cm are illustrated in Fig. 3.29. The figure shows that 83% electrons with kinetic energy higher than 2 MeV are located in the bunch within the length of about 35 ps. Electrons with lower energy than 2 MeV, which have large vertical position and large divergence will be filtered out by using energy slits inside the alpha magnet vacuum chamber. The electron beam is then directed to enter the linac at its centroid position with small divergence angle. If the electron beam entering the linac with off-axis position and large divergence angle, it will be kicked by a magnetic field component of the RF wave in the linac. This will result in electron colliding with the accelerating tube wall and off-axis acceleration.

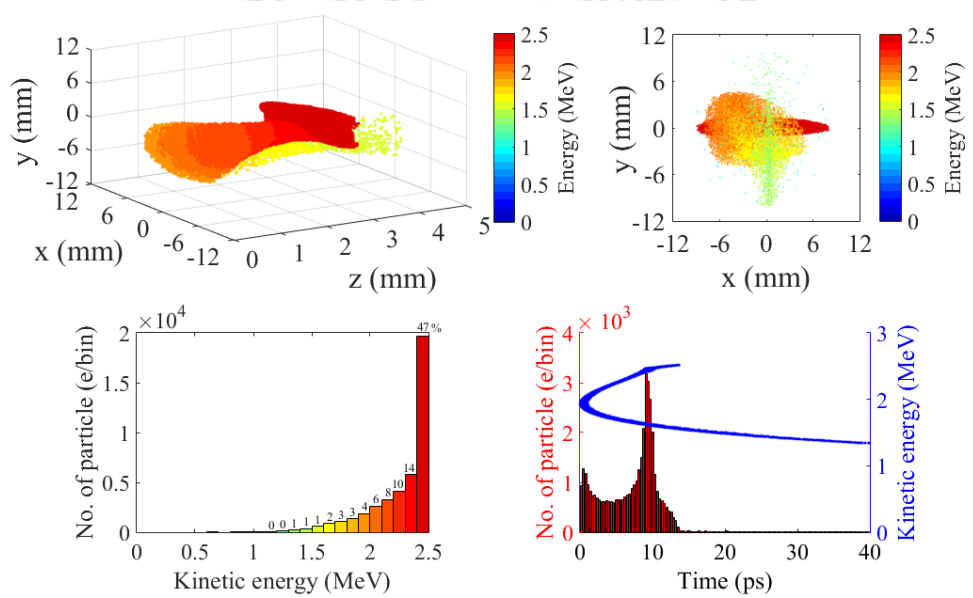

Figure 3.29: 3D particle distribution (top left), transverse beam distribution (top right), energy spectrum (bottom left) and energy-time phase space with histogram (bottom right) at the linac entrance for alpha magnet gradient of 300 G/cm without energy filter.

For PARMELA simulation in this section and the following, the maximum-energy electron is specified to be the reference particle. Consequently, this particle will experience a given linac RF phase, while other particles will experience either larger or smaller RF phase depending on their position in the bunch. If the given linac RF phase is 90° (on-crest phase), the reference particle will be accelerated in the linac and gain maximum kinetic energy. Other particles will arrive at the RF phase with lower electric field magnitude and gain less energy.

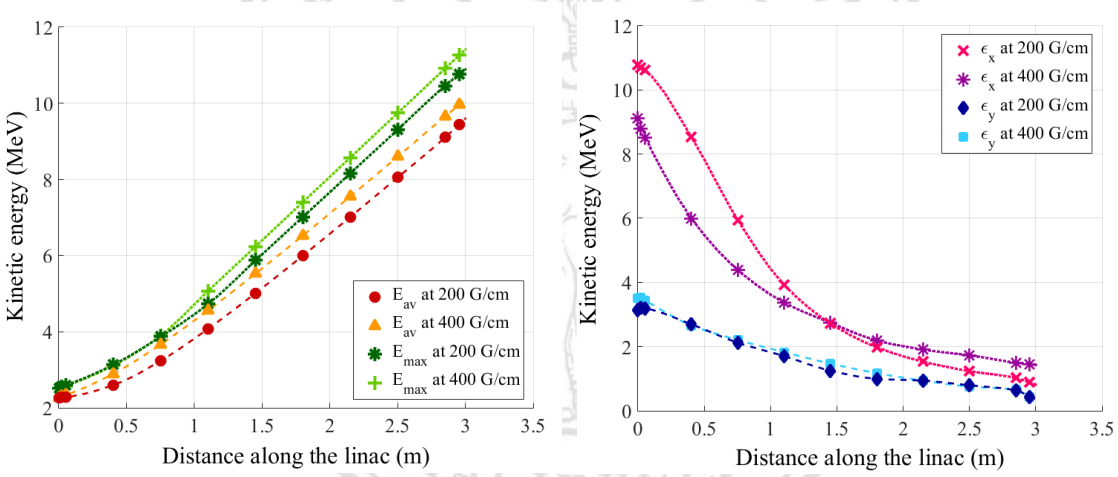

Figure 3.30: Average and maximum kinetic energies (left) and rms transverse emittance (right) of electron bunches, which are accelerated along the linac with a given RF phase of 90° for alpha magnet gradients of 200 G/cm and 400 G/cm.

The average axial electric field of 3.7 MV/m was set for the linac acceleration to reach the average beam energy after the linac exit of 9.81 MeV. The energy of electron beam increases continuously while travelling through the linac. As shown in Fig. 3.30 (left), energy of electron beam with larger alpha magnet gradient is higher since the electron bunch length at the linac entrance for this case is shorter. Hence, electrons in the bunch gains almost the same energy at nearly on-crest phase. In simulation, the quadrupole and steering magnetic fields were optimized to get the same transverse beam size before the beam entering the linac for different alpha magnet gradients. This leads to difference of the divergence angles and transverse beam emittances at the linac

entrance. When the electron bunch is accelerated through the linac, the transverse momentum reduces resulting in reduction of divergence angle and transverse emittance along the linac as shown in Fig 3.30 (right).

The energy of electron bunch after accelerated in the linac relies on several operating parameters such as electric field gradient, RF phase, RF frequency, beam loading effect, RF pulse width and the power dissipation in the linac wall. In this study, the beam loading effect, the RF pulse width and the power dissipation were not considered. The electron encountered with the sinusoidal electric field in the linac can be accelerated or decelerated depending on its arriving time with respect to the RF phase. In this section, the accelerating RF phase of the linac was surveyed to obtain a proper value for the optimization of the energy filtering in the next section. The linac RF phase was varied around the on-crest phase of 70° - 110° for the alpha magnet gradients of 200 to 400 G/cm without energy filter. The average energy and the energy spread of the electron bunch at the experimental station for various alpha magnet gradients are illustrated in Fig. 3.31. The transverse beam properties at the experimental station cannot be compared because different magnetic field strengths of quadrupole and steering magnets in the ATE section were applied to different alpha gradients and linac phases.

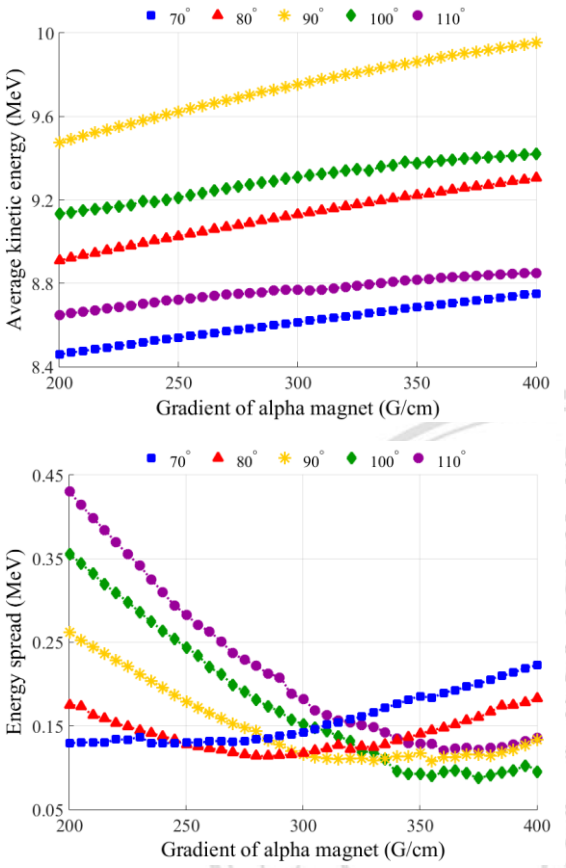

Figure 3.31: Average beam energy and energy spread at the experimental station as a function of alpha magnet gradient for the linac phases of 70°, 80°, 90°, 100°, and 110°.

At the on-crest acceleration with the phase of 90°, the electron bunch gains maximum energy at the crest of the sinusoidal electric field leading to the maximum average beam energy and minimum energy spread. The average energy of the electron bunch for the acceleration with the RF phase far from the on-crest condition is less due to smaller value of the electric field magnitude. Consequently, for the linac phase greater than 90°, low-energy electrons in the head of the bunch receive higher electric field amplitude than high-energy electrons in the tail. For the linac phase lower than 90°, the low-energy electrons obtain lower electric field amplitude than the high-energy electrons. This leads to the difference in average kinetic energies for different RF phases as shown in Fig. 3.31 (left). This effect is more significant with low alpha magnet gradient owing to longer electron bunch length at the linac entrance. The energy spread of electron bunch at the experimental station is minimum at different alpha magnet gradients for the same RF phase. The lower RF phase requires lower gradient to

achieve the minimum energy spread. The dependency of the linac RF phase on electron bunch length for different alpha magnet gradients at the experimental station are displayed in Figs. 3.32 and 3.33.

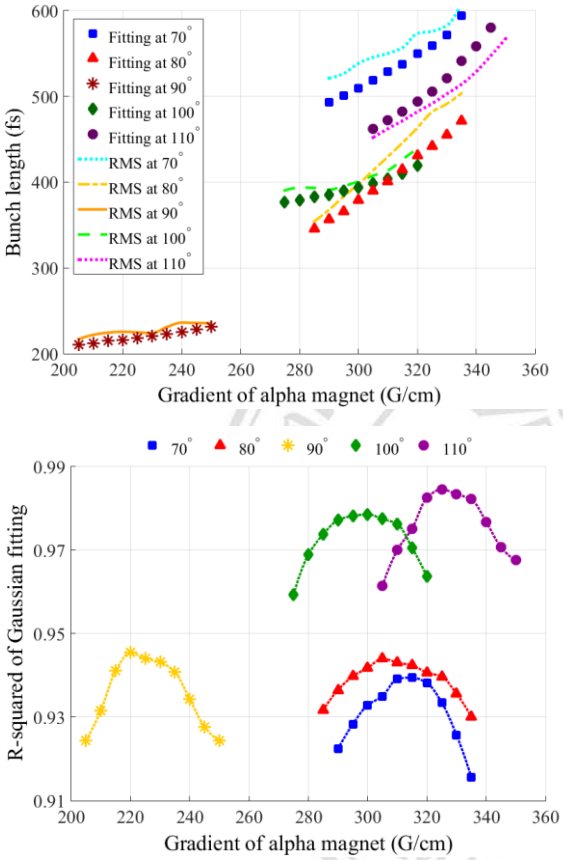

Figure 3.32: RMS bunch length, bunch length from Gaussian fitting (left) and R-squared value of the Gaussian fitting (right) at the experimental station as a function of the alpha magnet gradient for the linac RF phases of 70° - 110°.

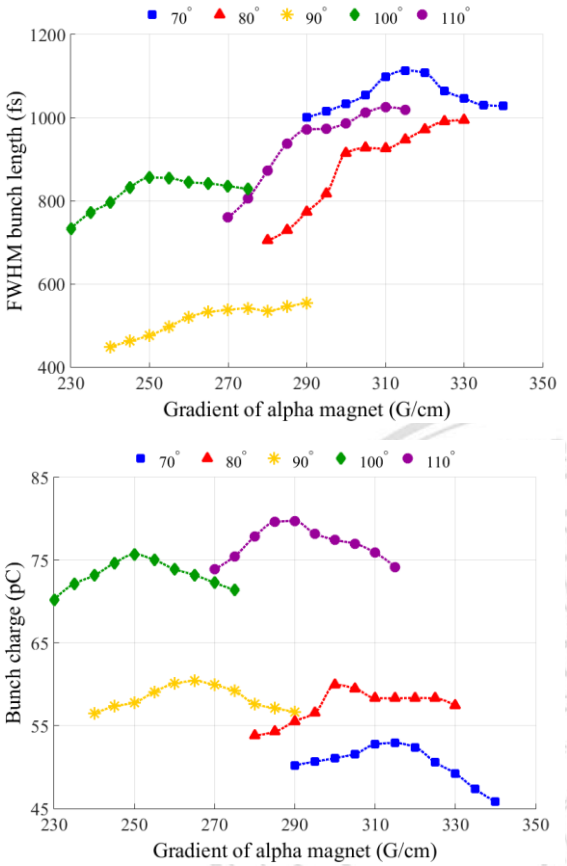

Figure 3.33: FWHM bunch length and electron bunch charge at the experimental station as a function of the alpha magnet gradient for the linac phases of 70° - 110°.

The Gaussian fitting bunch length and the rms bunch length show comparable values as shown in Figs. 3.27 and 3.32. The values of R-squared from the Gaussian fitting are in the range of 0.9 - 1, which guarantee the reliability of the fitting process. The rms, FWHM and Gaussian fitting bunch lengths at the experimental station are longer when the alpha magnet gradient increases. The maximum value of R-squared and electron bunch charge for each linac RF phase can be obtained at different alpha magnet gradients. The R-squared value for the RF phase of 90° is maximum at low alpha magnet gradient. Hence, the on-crest RF phase provides the shortest bunch lengths of the electron beam. For off-crest linac RF phase, the R-squared value is maximum at high alpha magnet gradient. Thus, the electron beam has longer bunch lengths at the experimental station. As the results, the proper linac RF phase for obtaining the electron beam with short bunch length at the experimental station is in the range of 80° - 100°.

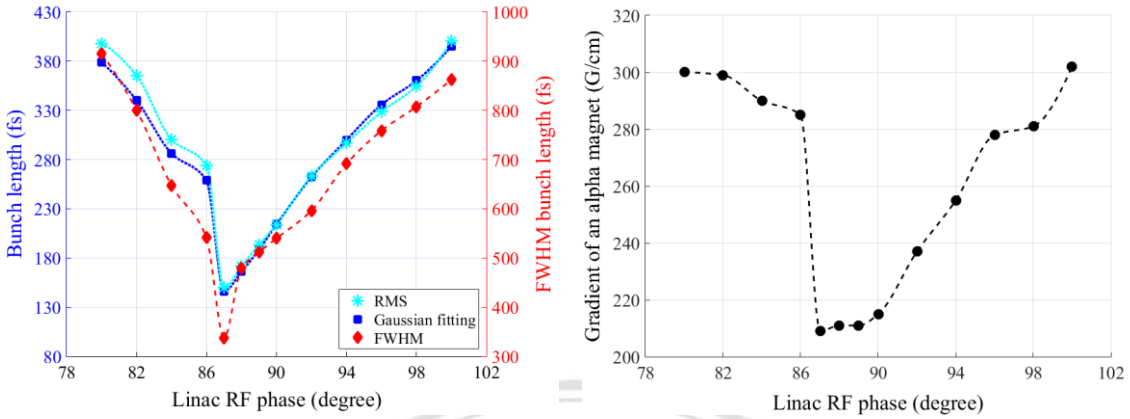

Figure 3.34: RMS, Gaussian fitting and FWHM bunch lengths of electron beams at experimental station versus linac RF phase in the range of 80° - 100° (left) and the relation between the optimal gradient of the alpha magnet and the linac RF phase (right).

Consequently, the linac RF phase was adjusted from 80° to 100° with a step of 2°. For each phase, the alpha magnet gradient was varied to obtain the minimum FWHM and rms bunch length as well as the maximum R-squared value for the Gaussian fitting bunch length. In this RF phase range, the Gaussian fitting and the rms bunch lengths are in the range of 140 - 400 fs, which is equivalent to the FWHM bunch lengths of 330 - 900 fs. The shortest bunch length is at the linac RF phase of 87° with the alpha magnet gradient of 209 G/cm. The minimum Gaussian fitting, rms and FWHM bunch lengths are 146, 150 and 337 fs, respectively.

3.3.5 Optimization of Energy Filtering

The main purpose of using energy slits inside the alpha magnet vacuum chamber is to filter out electrons with low energy before injecting the beam to the linac entrance. This was performed in order to filter out low-energy electrons in the long tail at the experimental station and to reduce the collision of low energy electrons with the linac wall. As a result, the X-ray production from Bremsstrahlung radiation is reduced. In this section, the energy filtering was studied to investigate the impact of energy spread on the compression of the longitudinal distribution of electron bunch in the linac. The transverse beam size at the linac entrance was controlled by using the quadrupoles and the steering magnets to have the beam size smaller than the aperture of the vacuum chamber in front of the linac, which has a radius of 10 mm. In this study, we used the

codes ELEGANT and PARMELA together to define the optimal condition of the energy filtering.

The energy filter feature of the alpha magnet in the code ELEGANT was divided into two parts, which are determined by inner and outer scrapers (DP1 and DP2). Both scrapers are associated with fractional momentum deviations and will be calculated to be the slits' horizontal position deviations. The inner scraper represents the low energy slit and was optimized to achieve the appropriate minimum energy of electron beam before exiting the alpha magnet. In this optimization, the linac phase was fixed at the optimum value of 87° with the optimum alpha magnet gradient of 209 G/cm. For comparison, the electron distributions at the alpha magnet exit without energy filtering are shown in Figs. 3.35 and 3.36. The inner scraper was varied to obtain the electron beam at the alpha magnet exit with energy range of 0.8 - 2.4 MeV. The magnetic fields of all quadrupoles and steering magnets in the GTA section were optimized to the proper values for different energy filters.

The properties of electron beam at the alpha magnet exit as a function of the minimum energy cut are shown in Fig. 3.37. The simulation results show that when the energy cut is larger than 1.4 MeV, the electron bunch charge decreases dramatically. At this energy cut, 94% of electrons in the bunch can exit the alpha magnet. Low-energy electrons cause bigger transverse size and larger divergence than high-energy electrons. Thus, optimization of electron filter was performed to obtain electron beam with small transverse beam size and small divergence. This will result in the reduction of the transverse beam emittance. When the value of minimum energy cut increases, the average beam energy exponentially increases and the energy spread exponentially decays.

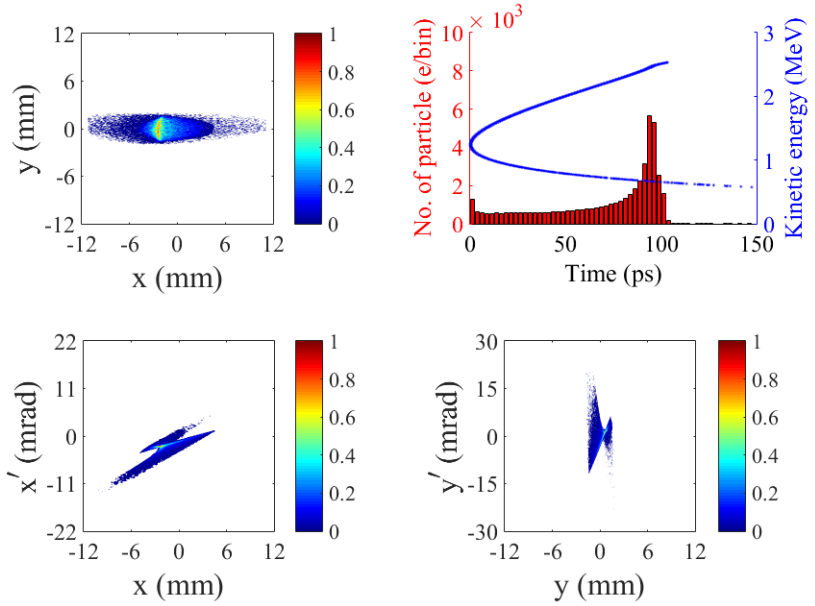

Figure 3.35: Transverse beam distributions (x-y), the energy-time phase space (E_k-t) with histogram and transverse phase space (x-x′ and y-y′) at the alpha magnet exit for the linac RF phase of 87° and the alpha magnet gradient of 209 G/cm without energy filter.

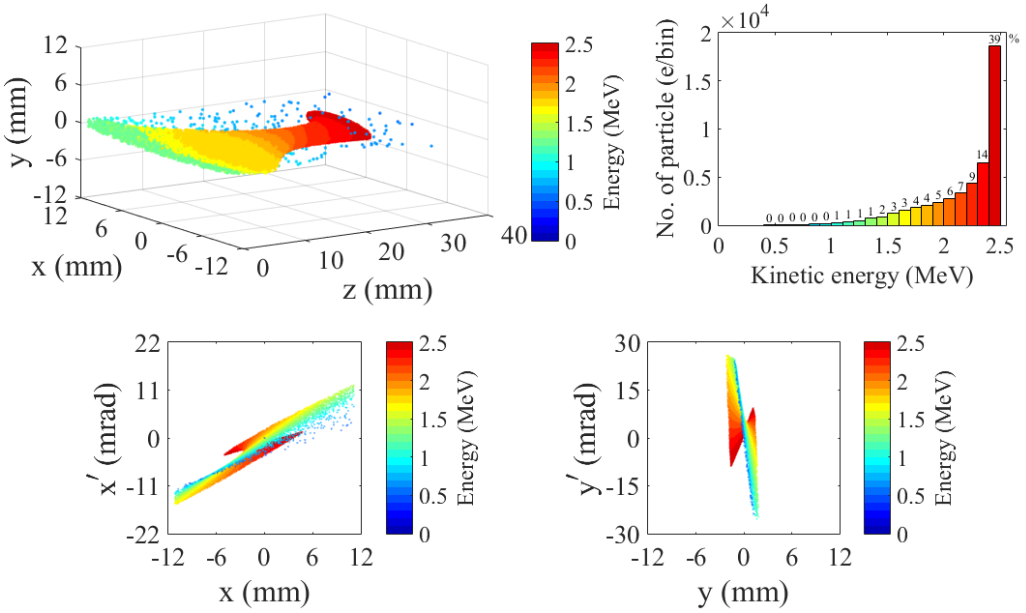

Figure 3.36: 3D electron beam distribution, energy spectrum and transverse phase space distributions (x-x′ and y-y′) at the alpha magnet exit for the linac RF phase of 87° and the alpha magnet gradient of 209 G/cm without energy filter.

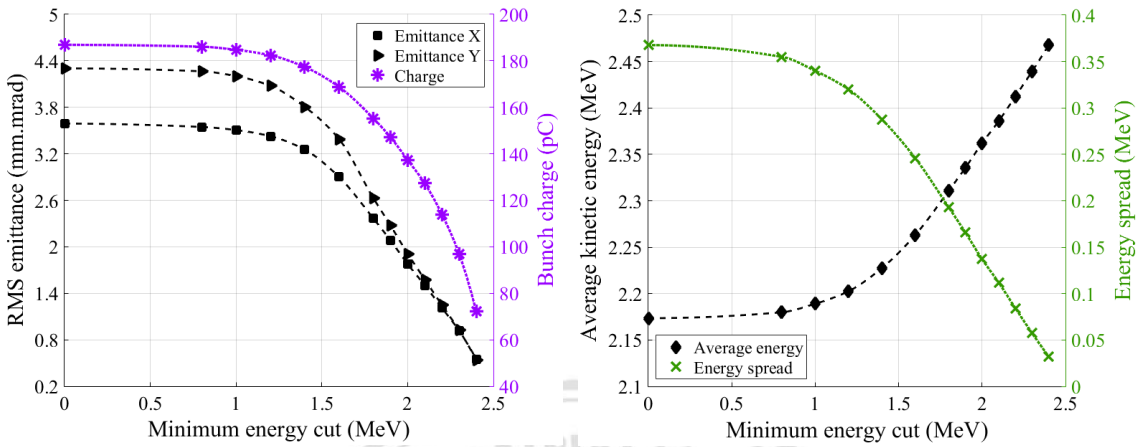

Figure 3.37: RMS transverse beam emittance, micro-bunch charge, average kinetic energy and energy spread of electron beam at the alpha magnet exit as a function of the minimum energy cut by using the energy slit inside the alpha magnet.

Beam dynamic simulation results in Fig. 3.38 show that most electrons, which are accelerated to the linac exit, have initial energy higher than 2 MeV. While lower energy electrons, which cause large transverse size and divergence, are lost in the linac. The vertical beam size at the linac exit after the acceleration is larger than the vacuum chamber. Some electrons with kinetic energy less than 9.7 MeV collide the wall at the linac exit. The number of lost particles starts to decrease while the energy cut is 2.4 MeV. The bunch charge of the remaining electrons at the linac exit for energy cut of 2.4 MeV is 72 pC, which is about half of total number of electrons at the linac entrance.

The quadrupole and steering magnets installed prior the linac are very crucial for the transverse beam distribution before and after the linac acceleration. In this simulation, we optimized all magnets to control the beam size to be smaller than the vacuum boundary at the linac exit. However, some electrons still strike with the chamber wall in either vertical or horizontal axis. Consequently, the magnets were employed to obtain the maximum bunch charge at the linac exit and the horizontal beam size was adjusted to be smaller than the chamber width.

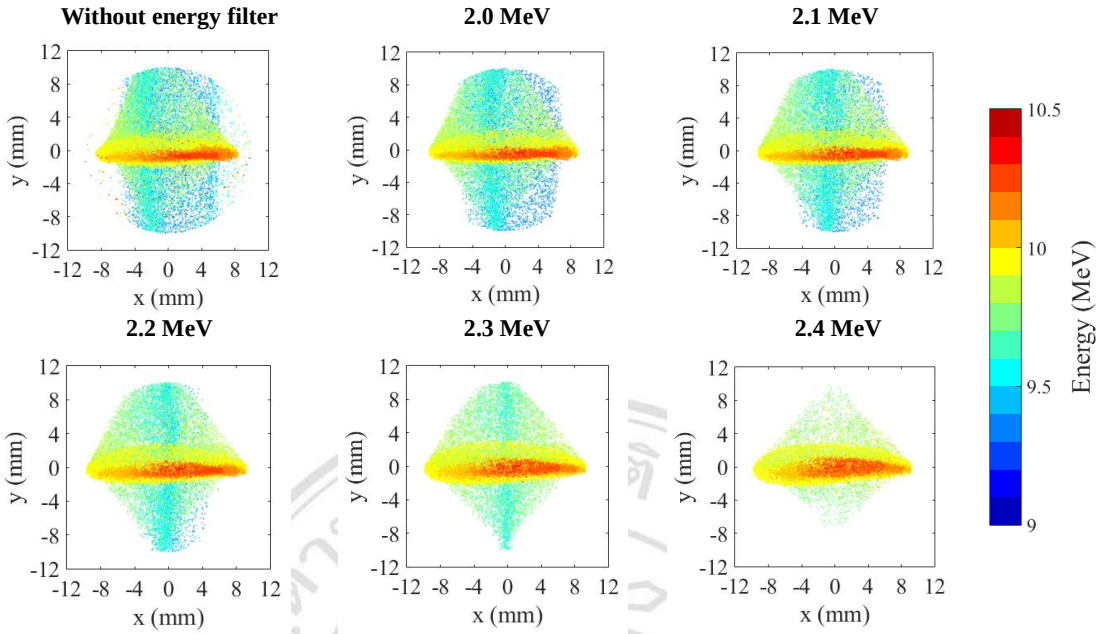

Figure 3.38: Transverse beam distributions at the linac exit for energy filter with different minimum energies.

The larger transverse beam size after the linac acceleration is not the effect from the space-charge forces since the electric and magnetic self-fields from electron beam with velocity close to the speed of light are cancelled [37]. The first argument for larger beam size is the kick force of the transverse RF magnetic field near the edge of the accelerating tube that affects significantly to off-axis electrons. In practice, wakefield effects can also be one of the reason to influence the transverse beam size in the linac. The wakefield is produced from the interaction between electric field of relativistic electrons and conducting-boundary discontinuities [13]. It induces the transverse deflection of electrons in the tail of the bunch resulting in larger beam size and consequently the beam loss on the linac wall. However, the wakefield effects were not included in this simulation.

In the experiments, the transverse size of the electron after the linac is smaller than the vacuum chamber because solenoid magnets were used along the accelerating tube as external focusing elements. These magnets were not included in the PARMELA simulation. These arguments reveal that both high and low energy electrons with off-axis position at the linac entrance can be deflected further from the central axis leading to the larger transverse beam distribution at the linac exit. Therefore, the transverse size and the transverse position of the electron before entering the linac should be optimized.

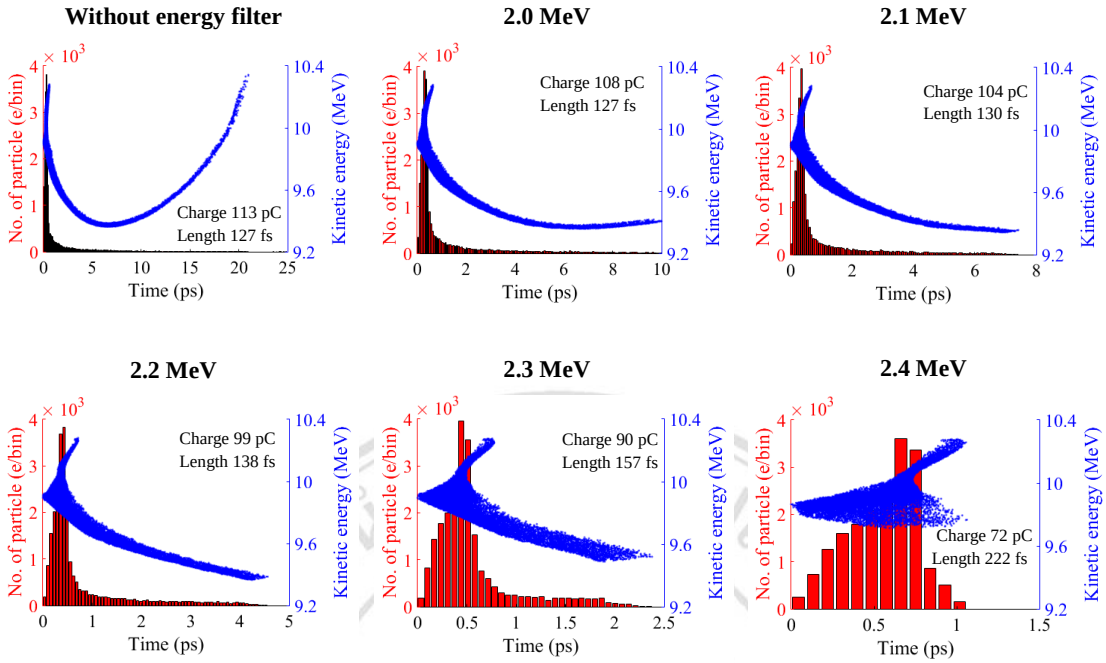

Figure 3.39: Energy-time phase spaces and histograms of macro-particles at the experimental station for energy filters in the range of 2.0 to 2.4 MeV compared to the case of without energy filter.

The electron beam departing from the linac was controlled by two quadrupole magnets to have the transverse size at the experimental station smaller than 10.5 mm. This is constrained by the size of the chamber aperture and the gap of the undulator magnet. Longitudinal beam distributions at the experimental station in Fig. 3.37 show that high-energy electrons are accumulated at the head of the bunch. The impact of the energy filter on the longitudinal phase space is well shown. The histograms of macro-particles in Fig. 3.39 show that low-energy electrons in the tail of the bunch can be filtered out at the energy greater than 2.3 MeV, while the Gaussian fitting bunch length of the electron beam increases as the minimum energy filter higher than 2.1 MeV. Thus, more optimization was performed by considering the distribution of electrons in the head of the bunch for the energy cuts of 2.1, 2.2, 2.3 and 2.4 MeV as displayed in Fig. 3.40. It shows that when the minimum energy filter is higher than 2.1 MeV, most electrons gradually shift from the head to the tail of the bunch.

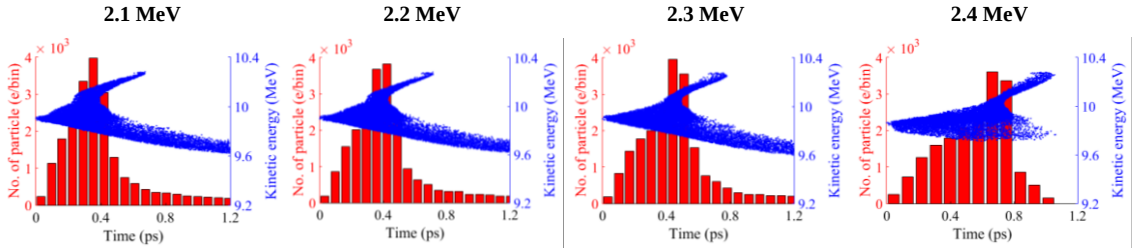

Figure 3.40: Longitudinal distributions and particle histograms of electrons concentrating in the head of the bunch at the experimental station for the energy filter with minimum energies of 2.1, 2.2, 2.3, and 2.4 MeV.

The optimal operating parameters of the PBP-CMU Linac system should produce electron beam with high bunch charge, low emittance and short bunch length at the experimental station. The optimization results show that the optimal RF phase is 87° with the alpha gradient of 209 G/cm and the minimum energy filter of 2.1 MeV. The transverse and longitudinal distributions as well as the 3D distribution of the electron bunch at the experimental station for optimal operating conditions are shown in Figs. 3.41 - 3.43. The Gaussian fitting bunch length was calculated to be 130 fs with the bunch charge of 104 pC. The energy spectrum of the electron bunch approaches the Gaussian distribution with energy spread of 0.21 MeV and half of electrons in the whole bunch occupies in the kinetic energy range of 9.8 - 10 MeV. As shown in Fig. 3.42, the divergence angle in y axis is larger than that in x axis because the vertical beam size at the linac exit is larger than the vacuum chamber. Thus, quadrupole magnets were used to strongly focus the beam in y direction. Thus, the vertical divergence increases up to 4.04 mrad at the experimental station, while the horizontal divergence is equal to 1.32 mrad. The transverse emittances are 0.81 and 0.65 mm.mrad for x and y axes, respectively.

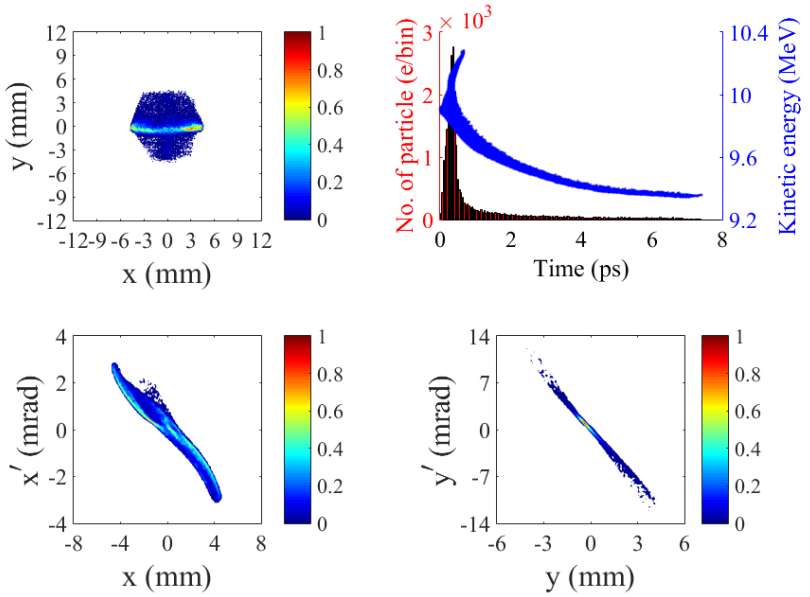

Figure 3.41: Transverse distribution, longitudinal phase space distribution with histogram of macro-particle number and transverse phase spaces of electron bunch at the experimental station for optimal operating parameters, which the linac RF phase is 87°, the alpha magnet gradient is 209 G/cm and the minimum energy filter is 2.1 MeV. Different colors in the plots represent different particle intensities in arbitrary unit.

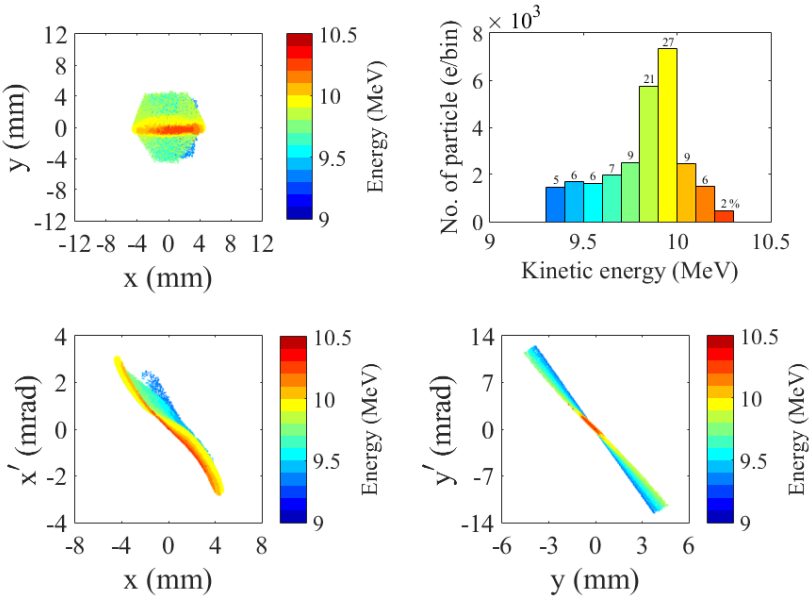

Figure 3.42: Transverse distribution, energy spectrum and transverse phase space distributions at the experimental station for optimal operating conditions, which the linac RF phase is 87°, the alpha magnet gradient is 209 G/cm and the minimum energy

filter is 2.1 MeV. Different colors in the plots represent the particles with different energies.

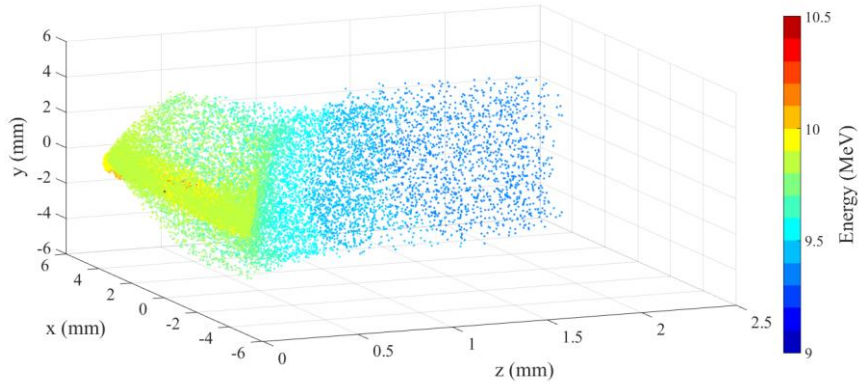

Figure 3.43: Three-dimensional electron beam distribution at the experimental station for optimal operating parameters, which the linac RF phase is 87°, the alpha magnet gradient is 209 G/cm and the minimum energy filter is 2.1 MeV.

3.4 Comparison of Measured Electron Beam Properties and Simulation Results

In this section, we consider three cases of operating parameters. The beam properties in the first case (Case 1) are obtained from the measurements [6]. The second case (Case 2) is the simulation with the same alpha magnet gradient and the minimum energy cut as in the experiment. The last case (Case 3) is the simulation with the optimal beam properties as described and discussed in Section 3.3. The considered operating parameters, which are alpha magnet gradient, minimum energy cut and linac RF phase, of the 3 cases are listed in Table 3.3.

Table 3.3: Operating parameters for 3 considered cases.

Operating parameter	Case 1	Case 2	Case 3
Gradient of the alpha magnet [G/cm]	328	328	209
Minimum energy cut [MeV]	1.42	1.42	2.10
Linac RF phase [degree]	no data	90	87

In the experiment [6], the average energy, energy spread and bunch charge of the electron beam were measured by using a dipole magnet and the Faraday cup at the end of the beamline. The measurement result (see Fig. 3.44) reveals that with the alpha-

magnet gradient of 328 G/cm and the minimal energy filter of 1.42 MeV, the average beam kinetic energy is 9.81 MeV with the energy spread of 1.09 MeV. The measured electron bunch charge is only 22.4 pC. These measured beam parameters are summarized in Table 3.4.

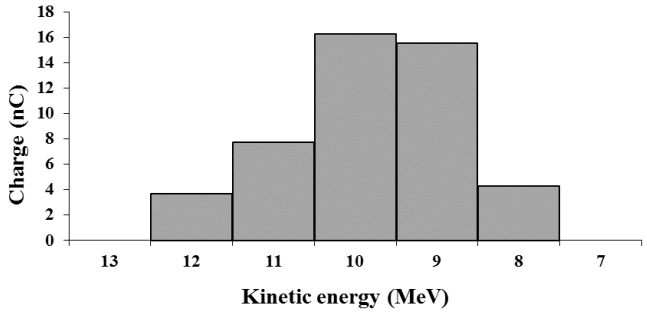

Figure 3.44: Measured kinetic energy and bunch charge of the electron beam after accelerating in the linac by using a dipole magnet and a Faraday cup [6].

The coherent transition radiation was generated at the experimental station. The electron bunch lengths of around 175 - 325 fs were measured with a Michelson interferometer when using the alpha magnet gradients of 250 - 410 G/cm. The experimental results are shown in Fig. 3.45.

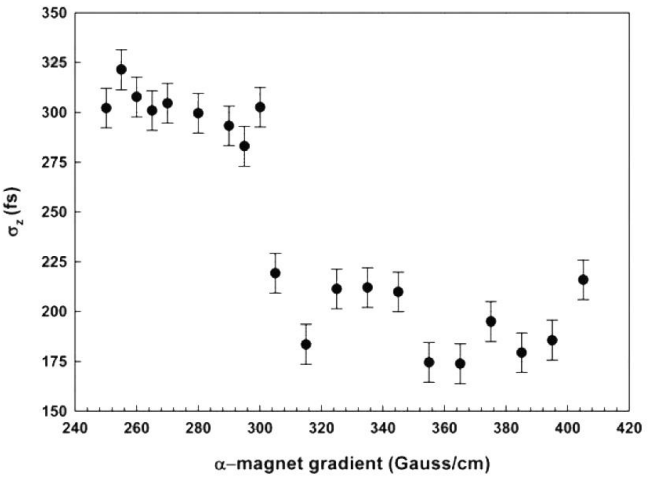

Figure 3.45: Measured electron bunch length at the experimental station as a function of the alpha magnet gradient [6].

Table 3.4: Measured properties of electron beam after accelerating in the linac [6].

Parameter	Value

Average energy [MeV]	9.81
Maximum energy [MeV]	12.00
Minimum energy [MeV]	8.00
Energy spread [MeV]	1.09
Gaussian fitting bunch length [fs]	200 - 225
Bunch charge [pC]	22.4

To study the beam dynamics of Case 2, which is the simulation with measured beam parameters, we applied the operating parameters in Table 3.3 in PARMELA simulation. Since the linac RF phase was not known in the experiment, the simulated RF phase of the linac in this case was fixed at the on-crest condition (90^o) to achieve the average beam energy of about 9.81 MeV. The simulation results for both transverse and longitudinal properties of the electron beam at the experimental station for Case 2 and Case 3 are listed in Table 3.5. It is noted that the measured electron beam properties in Case 1 show that the measured beam has shorter bunch length than Case 2 but longer than Case 3. It also has much less bunch charge than Case 2 and 3. This might come from the inefficient beam transportation along the accelerator system.

Figures 3.46 - 3.48 present the transverse and longitudinal distributions as well as the 3D beam distribution at the experimental station of Case 2. The transverse beam size is limited by the gap of the undulator magnet. The energy spectrum implies that 89% of the total electrons in the bunch are concentrated in the kinetic energy range of 9.7 - 9.9 MeV. This results in a very low energy spread of 0.09 MeV. The horizontal and vertical emittances are 1.25 and 0.49 mm.mrad, respectively. Similar plots for Case 3 are already shown in Figs. 3.41 - 3.43. The beam parameters of all 3 cases are used to calculate the undulator radiation power as described and discussed in Chapter 4.

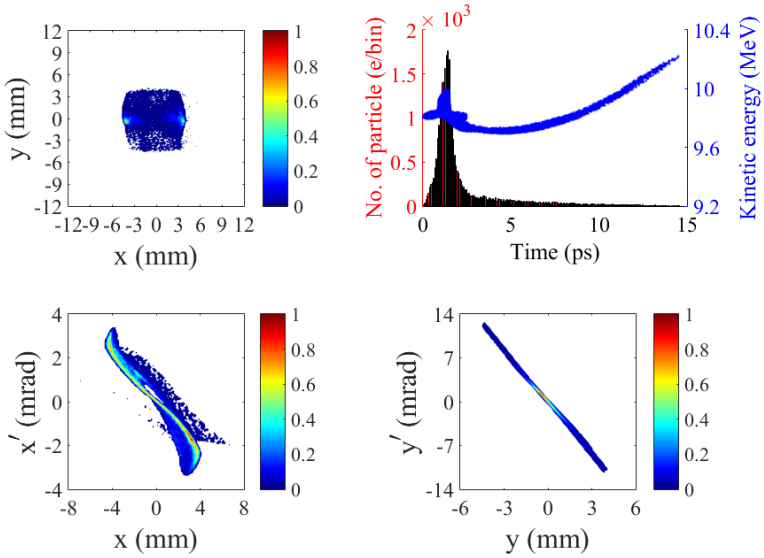

Figure 3.46: Contour plots of transverse beam distribution (x-y), longitudinal phase space (E_k-t) with histogram of the number of macro-particles and transverse phase space distributions (x-x′ and y-y′) at the experimental station for simulated beam of Case 2.

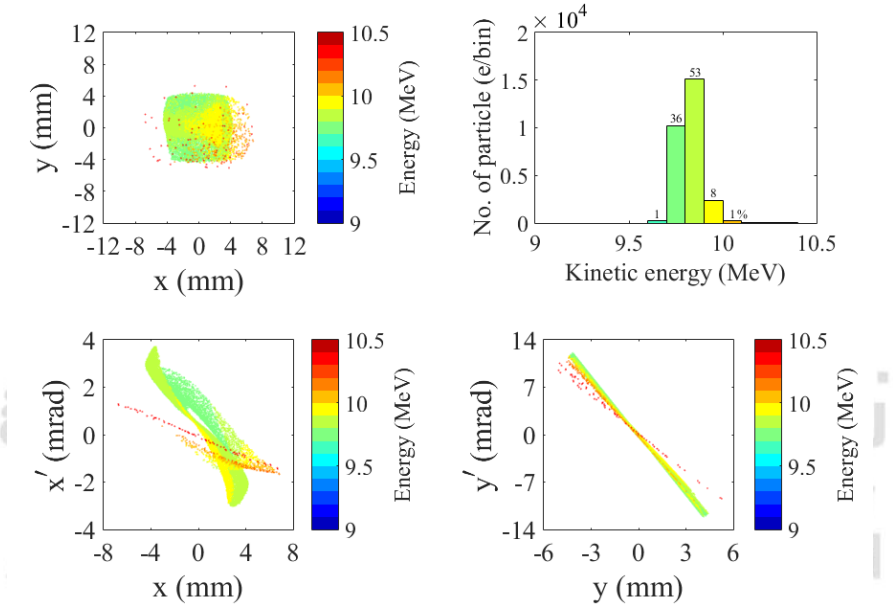

Figure 3.47: Transverse distribution (x-y), energy spectrum and transverse phase space distributions (x-x′ and y-y′) at the experimental station for simulated beam of Case 2. Different colors in the plots represent the particles with different energies.

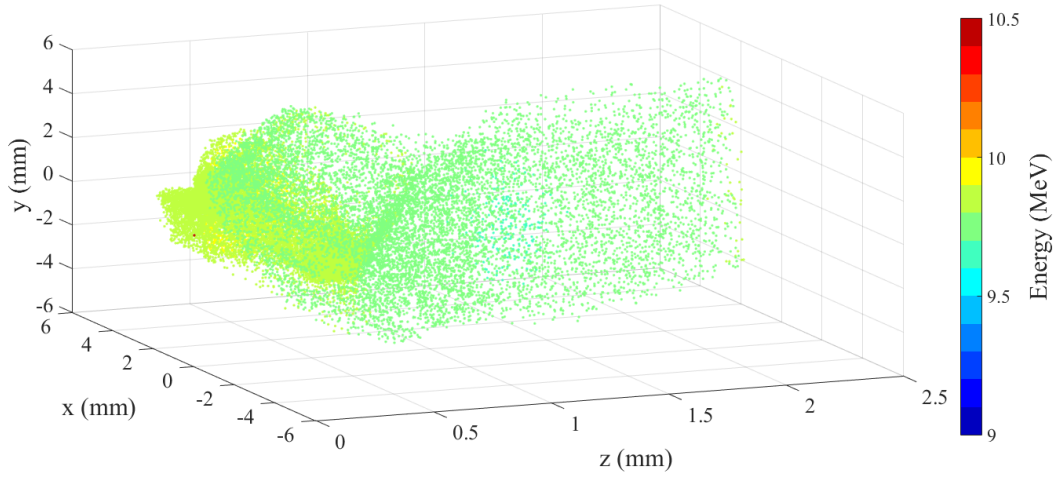

Figure 3.48: Three-dimensional electron beam distribution at the experimental station for simulated beam of Case 2. Different colors in the plots represent the particles with different energies.

Table 3.5: Operating parameters and simulated electron beam properties at the experimental station for simulation of Case 2 and Case 3.

Operating parameter	**Case 2**	**Case 3**
Gradient of alpha magnet [G/cm]	328	209
Minimum energy cut [MeV]	1.42	2.10
Linac RF phase [degree]	90	87
Transverse property		
Beam size x [mm]	2.76	2.54
Beam size y [mm]	1.65	1.48
Divergence x [mrad]	1.73	1.32
Divergence y [mrad]	4.48	4.04
Emittance x [mm.mrad]	1.25	0.81
Emittance y [mm.mrad]	0.49	0.65
Longitudinal property		
Average energy [MeV]	9.82	9.82
Maximum energy [MeV]	11.14	10.28
Minimum energy [MeV]	9.69	9.34

Energy spread [MeV]	0.09	0.21
RMS bunch length [fs]	442	135
Gaussian fitting bunch length [fs]	386	130
FWHM bunch length [fs]	767	266
Bunch charge [pC]	110.4	104.4